PL-TR--92-1053

PL-TR--
92-1053

(2)

VORTEX SHEDDING BY BLUNT/BLUFF BODIES AT HIGH REYNOLDS NUMBERS

Volume I of IV
Data Analysis

B. R. Merrill

March 1993

Final Report

PHILLIPS LABORATORY
Directorate of Plans and Programs
AIR FORCE MATERIEL COMMAND
KIRTLAND AIR FORCE BASE, NM 87117-5776

PL-TR-92-1053, Vol I of IV

This final report was prepared by the Phillips Laboratory, Kirtland Air Force Base, New Mexico, under Job Order 9993XX21. The Laboratory Project Officer-in-Charge was Bruce R. Merrill (XPXS).

When Government drawings, specifications, or other data are used for any purpose other than in connection with a definitely Government-related procurement, the United States Government incurs no responsibility or any obligation whatsoever. The fact that the Government may have formulated or in any way supplied the said drawings, specifications, or other data, is not to be regarded by implication, or otherwise in any manner construed, as licensing the holder, or any other person or corporation; or as conveying any rights or permission to manufacture, use, or sell any patented invention that may in any way be related thereto.

This report has been authored by an employee of the United States Government. Accordingly, the United States Government retains a nonexclusive royalty-free license to publish or reproduce the material contained herein, or allow others to do so, for the United States Government purposes.

This report has been reviewed by the Public Affairs Office and is releasable to the National Technical Information Service (NTIS). At NTIS, it will be available to the general public, including foreign nationals.

If your address has changed, if you wish to be removed from our mailing list, or if your organization no longer employs the addressee, please notify PL/XPXS, Kirtland AFB, NM 87117-5776 to help us maintain a current mailing list.

This report has been reviewed and is approved for publication.

Bruce R. Merrill
BRUCE R. MERRILL, GS-14
Project Officer

FOR THE COMMANDER

Michael C Dieckhoff
MICHAEL C. DIECKHOFF, GM-15
Chief, Studies and Analysis
Branch

MICHAEL E. HAVEY, Col, USAF
Director, Plans and Programs
Directorate

DO NOT RETURN COPIES OF THIS REPORT UNLESS CONTRACTUAL OBLIGATIONS OR NOTICE ON A SPECIFIC DOCUMENT REQUIRES THAT IT BE RETURNED.

REPORT DOCUMENTATION PAGE

1. AGENCY USE ONLY (Leave blank)	2. REPORT DATE	3. REPORT TYPE AND DATES COVERED
	March 1993	17 Jun 91-31 Jul 92

4. TITLE AND SUBTITLE

VORTEX SHEDDING BY BLUNT/BLUFF BODIES AT HIGH REYNOLDS NUMBERS, Volume I of IV-Data Analysis

PE: 62601F
PR: 9993
TA: XX
WU: 21

6. AUTHOR(S)

B. R. Merrill

7. PERFORMING ORGANIZATION NAME(S) AND ADDRESS(ES)

Phillips Laboratory
Kirtland AFB, NM 87117-6008

PL-TR--92-1053

9. SPONSORING/MONITORING AGENCY NAME(S) AND ADDRESS(ES)

10. SPONSORING/MONITORING AGENCY REPORT NUMBER

11. SUPPLEMENTARY NOTES

12a. DISTRIBUTION/AVAILABILITY STATEMENT

Approved for public release: distribution is unlimited.

12b. DISTRIBUTION CODE

13. ABSTRACT (Maximum 200 words)

This report documents the analysis of vortex shedding data collected by the Phillips Laboratory at the U.S. Air Force Academy Subsonic Wind Tunnel facility. The analysis is primarily of the power spectrum of the vortex shedding as seen in the force and moment coefficient power spectra. The shedding frequencies as seen in the power spectra are used to analyze for the Strouhal number. The analysis suggests that shape and orientation in the wind field have an effect on the shedding of vortices.

14. SUBJECT TERMS

Vortex shedding, Vortices, Aerodynamic forces, Coefficients, Drag, Strouhal number

15. NUMBER OF PAGES

54

17. SECURITY CLASSIFICATION OF REPORT	18. SECURITY CLASSIFICATION OF THIS PAGE	19. SECURITY CLASSIFICATION OF ABSTRACT	20. LIMITATION OF ABSTRACT
Unclassified	Unclassified	Unclassified	SAR

NSN 7540-01-280-5500

ACKNOWLEDGMENT

The author would like to acknowledge the many useful discussions with Dr. Paul Merritt and Mr. Kerry Sandstrom. Throughout the analysis effort they provided insight into and suggestions for the data analysis and the interpretations drawn from it. The author would also like to thank Capt Gregory Gates, the experimental team leader, both for making the data available and for patiently explaining the experimental setup and the data collection procedures. In spite of this help, any and all errors in this report are the sole responsibility of the author.

CONTENTS

FIGURES

FIGURES (Concluded)

TABLES

1.0 INTRODUCTION

This report documents the analysis of vortex shedding data collected by the Phillips Laboratory at the U.S. Air Force Academy Subsonic Wind Tunnel facility. A preliminary examination of the USAF Academy data was presented by Jumper et.al. (Ref. 1). The purpose of this report is to more fully examine the data and present this analysis. The analysis is primarily of the power spectrum of the vortex shedding as seen in the force and moment coefficient power spectra. The shedding frequencies as determined from the power spectra are used to analyze for the Strouhal number. The average values of force and moment coefficients are also presented. This report covers a large number of test objects with different shapes subjected to varying wind speeds. The tunnel wind speeds were selected to simulate 15- to 45-mph winds on 1- to 3-m telescope sizes of similar shapes. Reynolds numbers of interest are generally in the region from 10^5 to 10^6. Additional analyses which may prove useful are suggested.

The Phillips Laboratory is involved in several programs which will make use of large telescopes. To successfully design a telescope system one must understand the possible causes of jitter. One important source is aerodynamic loading. Of interest here are those loads induced by vortex shedding brought about by the flow of air over the structure. The data presented in this report show that the shape of the test object is significant in determining if shedding will occur. This report considers the data good if distinct shedding was measured. However, the fact that telescope designers may intentionally select shapes that do not shed in order to minimize wind loading problems is taken into consideration. This report provides data for a designer to calculate mean forces and moments and the standard deviation of the fluctuating loads for a wide variety of shapes. No attempt is made to indicate telescope jitter levels caused by these loads. The designer must use structural and control system models for the specific system/shape to obtain these jitter estimates.

Recent studies of vortex shedding have added much to the body of knowledge regarding the shedding phenomena but have generally been conducted at Reynolds numbers below those of interest to the laboratory. In their review paper Griffin and Hall (Ref. 2) indicate that much of the recent work has been at Reynolds numbers of a few thousand or less with some occasional work at a few tens of thousands. Roshko (Ref. 3) reported on experimental data in the Reynolds number range of interest (10^5 to 10^6). Roshko's experiment used an 18-in diameter circular cross section cylinder which spanned the entire 8.5-ft height of the wind tunnel. Thus, there seems to be little data available regarding blunt/buff bodies at Reynolds numbers near 10^6.

The sheer volume of data analyzed precludes it from being contained all in one volume. Therefore this report is organized into a summary volume and three data volumes. This summary volume consists of a brief review of the experimental arrangement (Section 2.0),

An overview of the analysis methodology (Section 3.0), significant results of the analysis (Section 4.0), and conclusions and recommendations for additional analysis (Section 5.0). The Data Volumes contain the plots of the mean coefficients and the power spectra for cylinders, octagons, hexagons, (Data Volume II), cubes (Data Volume III), and rectangles (Data Volume IV).

2.0 EXPERIMENTAL ARRANGEMENT

The experimental arrangement has been described by Jumper et.al. (Ref. 1) and only a few salient features will be repeated here. The test objects, consisting of cubic, rectangular, and circular cylinders at varying inclination angles were positioned on a vertically pointing sting. The sting and test object were able to rotate in azimuth to simulate changing wind directions. The sting provided three-dimensional forces and moments acting on the test object. The sting data were sampled 740 times per second yielding a Nyquist frequency of 370 Hz. For each test object configuration (inclination, azimuth, and wind speed) 2048 samples were taken for Fourier analysis during a time period of 2.77 s. The inclination and azimuthal angles were defined as indicated in Figure 1. Tunnel wind speeds were nominally 60, 90, 120, and 180 ft/s. Tunnel wind speed was selected by controlling the tunnel fan speed.

This report covers 113 combinations of test shape, declination, and azimuth angle. For each of these combinations there are 24 measurements, including wind speed (4), and force and moment (6). Thus, over 2700 data sets were taken for analysis. The data were taken and archived on 5.25-in 360K floppy disks. These disks are now located in the Studies and Analyses Branch of the Plans and Programs Directorate at Phillips Laboratory. During this analysis some of the disks were found to have corrupted data sectors and consequently some data have been lost.

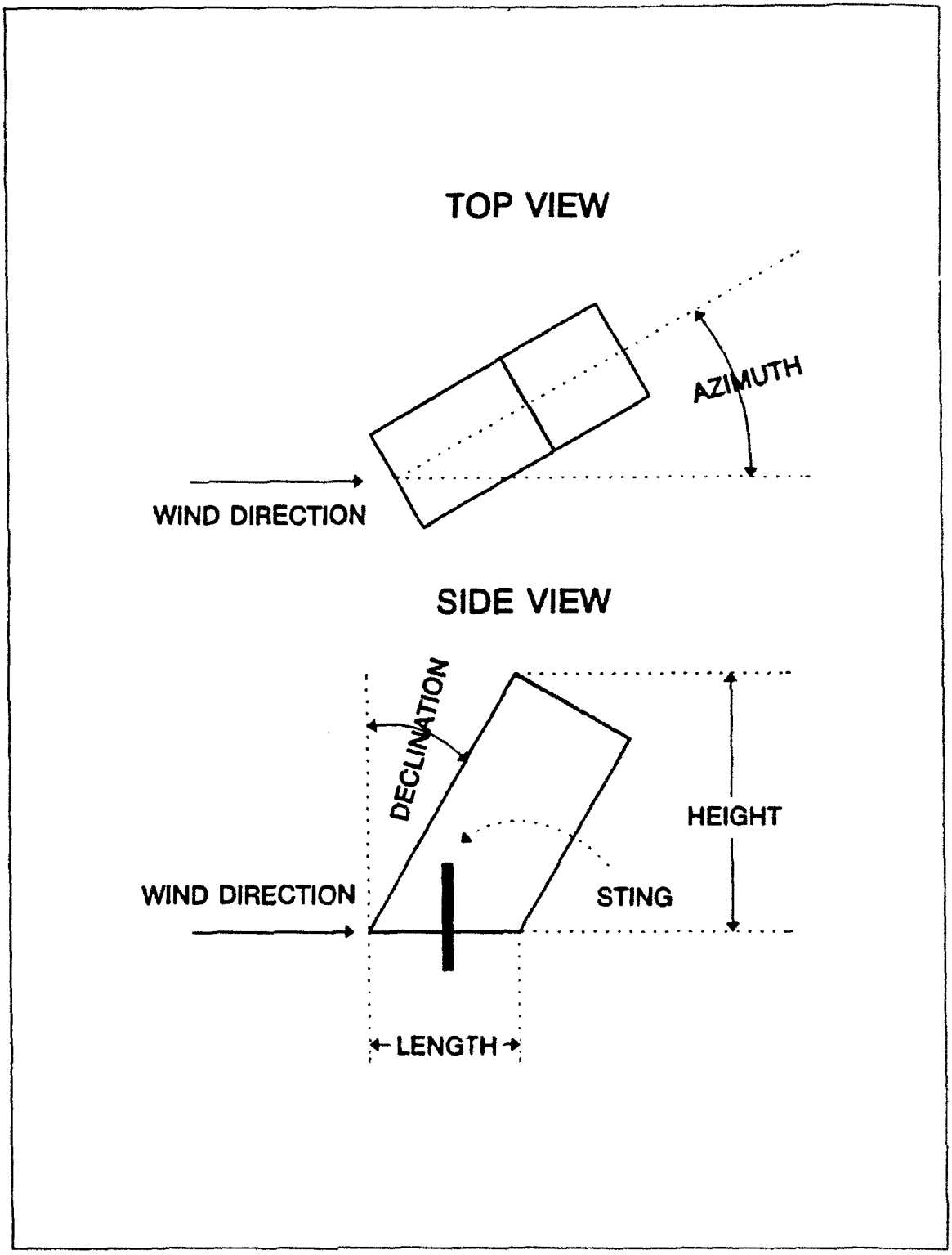

Figure 1. Test setup configuration.

3.0 DATA ANALYSIS

The sting used to make the force/moment measurements is shown in Figure 2. With respect to a coordinate system fixed to the sting there were two forces measured in each of the principle directions, a twisting moment around the vertical axis, and a vertical force. As the sting and test article were rotated in the wind tunnel, the coordinate system fixed to the sting rotated with respect to the wind tunnel. For this analysis all calculations are done with respect to the sting's coordinate system and no attempt was made to transform the measurements to a coordinate system fixed with respect to the tunnel. The three principle axes with respect to the sting were referred to as normal, lateral, and vertical. In Figure 2 forces F_1 and F_2 were along the normal axes, and F_3 and F_4 were along the lateral axis. The total normal force, F_n, and the total lateral force, F_l, were calculated as

$$F_n = F_1 + F_2$$

$$F_l = F_3 + F_4$$

The moments caused by the normal and lateral forces were calculated about the base of the sting as

$$M_n = [F_1 * (\tfrac{1}{2} l_{s_{1-2}} + l_e) + F_2 * (l_e - \tfrac{1}{2} l_{s_{1-2}})]$$

$$M_l = [F_3 * (\tfrac{1}{2} l_{s_{3-4}} + l_e) + F_4 * (l_e - \tfrac{1}{2} l_{s_{3-4}})]$$

where the moment arms are as shown in Figure 2.

A customary practice in aerodynamic analysis is to present force and moment coefficients rather than the actual forces and moments. The force and moment coefficients were calculated as

$$F_c = \frac{F}{\frac{1}{2} \rho v^2 A}$$

$$M_c = \frac{M}{\frac{1}{2} \rho v^2 A \frac{h}{2}}$$

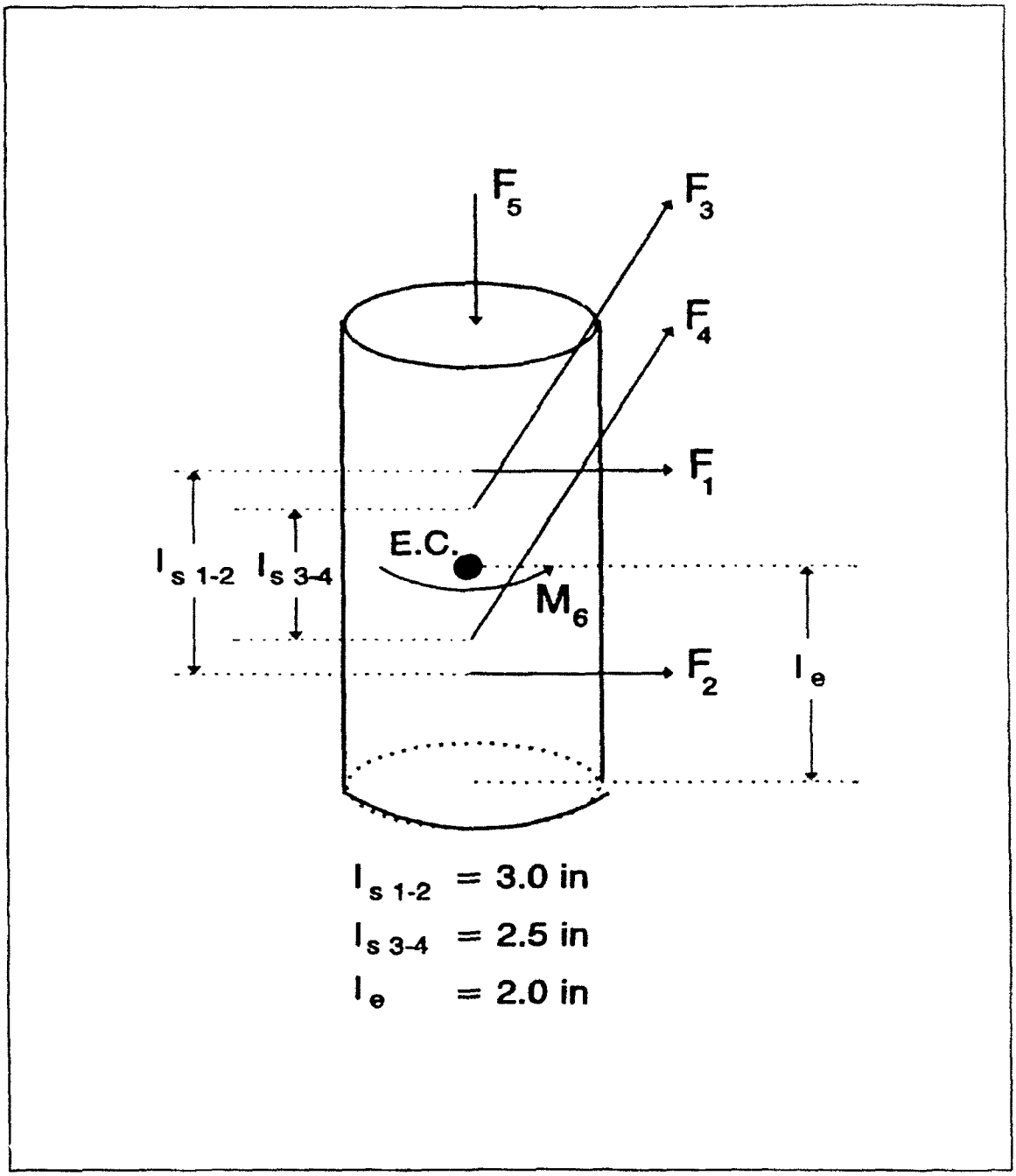

Figure 2. Sting Schematic. Forces and moments measured by the sting with respect to the electronic center (E.C).

where

F_c and M_c are the force and moment coefficients respectively
F and M are the forces and moments respectively and can be either F_n, F_l, M_n, or M_l
ρ is the air density
v is the air velocity
A is the frontal cross-sectional area, based on starting position. This area is used even when the object is rotated. The area is computed as the product of the width and height as reported in Table 1.
h is the height of the test object.

Although the test was conducted over a period of time when pressure and temperature conditions varied, a constant air density

$$\rho = 0.00188388 \frac{lbf\text{-}s^2}{ft^4}$$

was assumed.

The air velocities were the nominal values of 60, 90, 120, and 180 ft/s.

As the test object rotated in the wind tunnel the cross-sectional area presented to the wind changed. No attempt was made to account for the varying area in computing the force and moment coefficients during the initial analysis. Subsequent analysis showed that accounting for the varying area can be useful and this will be discussed later.

Measurements of the force along the vertical axis and the moment about the vertical axis were also made. The force data were not analyzed. The moment coefficient about the vertical axis was calculated using the measured moment normalized by the same factor used for the other two principle axes. After the analysis was complete it was realized that the moment measured by the sting was in units of inch-pound and the normalizing factor was in foot-pound. As a result of this error the moment coefficients calculated about the vertical axis were dimensional and actually have units of inch/foot. A note to this effect is included in the data volumes.

Several levels of processing were performed on the data. The raw voltage data were converted to forces and moment units and were grouped into individual files of 2048 data points prior to this analysis effort. For this analysis the forces and moment data were converted to coefficients as indicated above. The coefficient data were then processed to calculate the mean and then removed after which the remaining data were processed to determine the power spectra. The power spectra plots were then analyzed for vortex shedding signatures. Where distinctive signatures were found further analyses were carried out to determine the Strouhal number and the force and moment shedding coefficients.

Table 1. Test object physical characteristics.

SHAPE	DECLINATION (degrees)	DIMENSIONS LxWxH (in)	WEIGHT (grams)	TORSION FREQ (Hz)	NORMAL FREQ (Hz)	LATERAL FREQ (Hz)
CYLINDER	0	8.1 x 8.1 x 10.0	1130.5			
CYLINDER	0	8.1 x 8.1 x 8.0	1029.5	50	70	66
CYLINDER	30	8.99 x 8.08 x 8.99	898.1	39	70	88
CYLINDER	45	11.12 x 8.12 x 8.46	897.0	38	75	100
OCTAGON	0	8.0 x 8.0 x 10.0	1659.3	46	51	51
HEXAGON	0	8.0 x 8.0 x 10.0	1615.0	48	52	51
CUBE	0	7.64 x 7.9 x 6.03	735.5	45	89	83
CUBE	0	7.66 x 7.91 x 7.91	873.8	40	69	69
CUBE	0	7.62 x 7.88 x 9.56	1009.5	30	43	46
CUBE	30	9.0 x 7.7 x 8.5	951.1	34	65	81
CUBE	45	11.1 x 7.88 x 8.31	1029.5	30	61	81
R'ND CUBE	0	8.0 x 8.0 x 10.0	1700.0	34	46	46
R'ND CUBE	30	9.0 x 8.0 x 8.9	1575.4	36	61	74
RECTANG	0	3.9 x 7.9 x 7.76	691.1	69	81	86
RECTANG	0	4.06 x 8.0 x 4.0	925.9	60	105	101
RECTANG	30	9.13 x 4.06 x 8.69	755.8	50	78	110
RECTANG	30	4.54 x 7.96 x 4.46	750.9	98	116	111
RECTANG	45	11.4 x 3.92 x 8.5	695.0	44	79	121

4.0 RESULTS

As a way of introducing the data contained in the data volumes this section will discuss the data of the rectangle at a declination of 30 deg and 4.5-in height. In analyzing the data it was necessary to choose between two possible coordinate systems: one fixed with respect to the wind tunnel and the other fixed with respect to the test object. Since the test object was securely mounted to the sting and since the sting was rotated with the test object in the tunnel, the coordinate system fixed with respect to the test object required less calculations to reduce the data. For this reason, the coordinate system fixed with respect to the test object was chosen.

The terms wind direction, azimuth, normal, lateral, yaw, roll, and theta are used throughout the report and in the data volumes. A discussion of what is meant by these terms will help avoid confusion. The term wind direction has two meanings in this report; it may be the wind direction coming down the tunnel or, in the case of the test object based coordinate system, the apparent wind direction is identical with the azimuthal angle as measured from a wind tunnel based coordinate system. As used in discussions of data and on the graphs presenting the data in this report and in the data volumes the term wind direction and azimuth are identical. A wind direction of 0 deg means that the azimuthal angle shown in Figure 1 is also 0 deg. When the wind direction is 0 deg (or 180 deg) the direction of the "normal" forces sensed by the sting and the direction of the wind are collinear. The "lateral" forces are always perpendicular to the "normal" forces. When the wind direction is 90 deg then the direction of the "normal" forces and the wind direction are perpendicular. The terms yaw and lateral have the same meaning. The use of the word "yaw" is related to the conventional use and mounting of a sting in the wind tunnel. Likewise, the term "roll" is related to the conventional use of the sting. As used in this report roll refers to a moment about the vertical axis. Theta is the angular measurement synonymous with the declination angle shown in Figure 1.

4.1 MEAN

The mean force and moment coefficients are shown in Figures 3 through 7. Figures 3 through 7 each contain four plots, one for each of the four tunnel wind speeds. These wind speeds are indicated by their corresponding Reynolds numbers

$$R_e = \frac{V l \rho}{\mu}$$

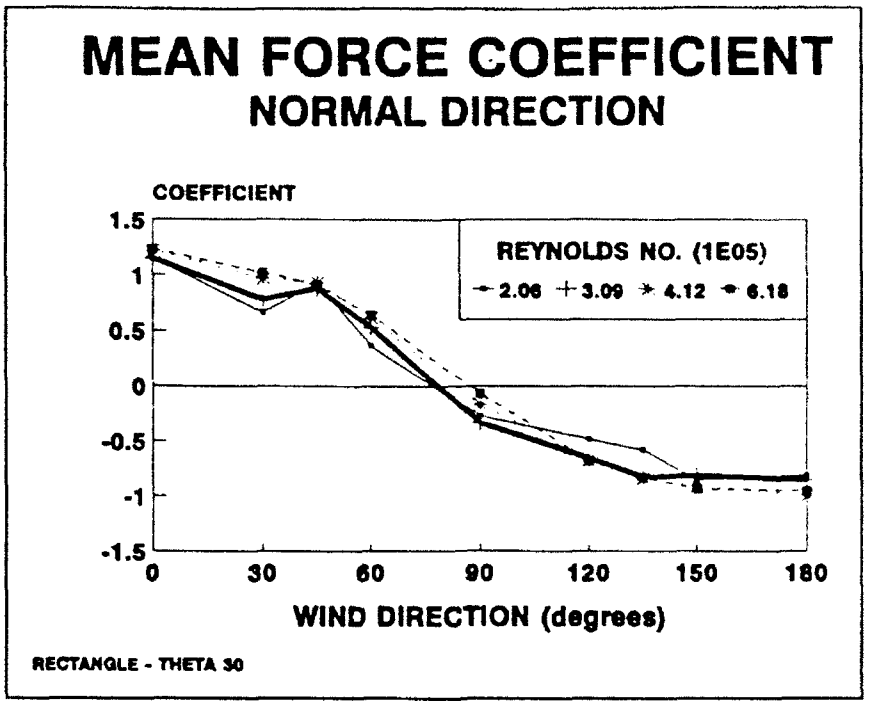

Figure 3. Mean force coefficient in the normal direction.

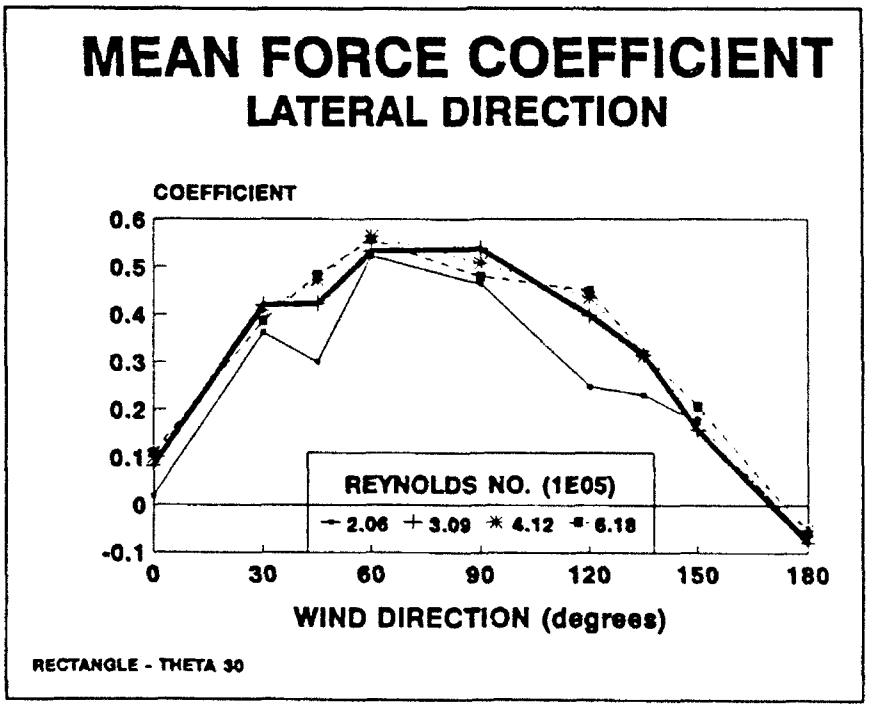

Figure 4. Mean force coefficient in the lateral direction.

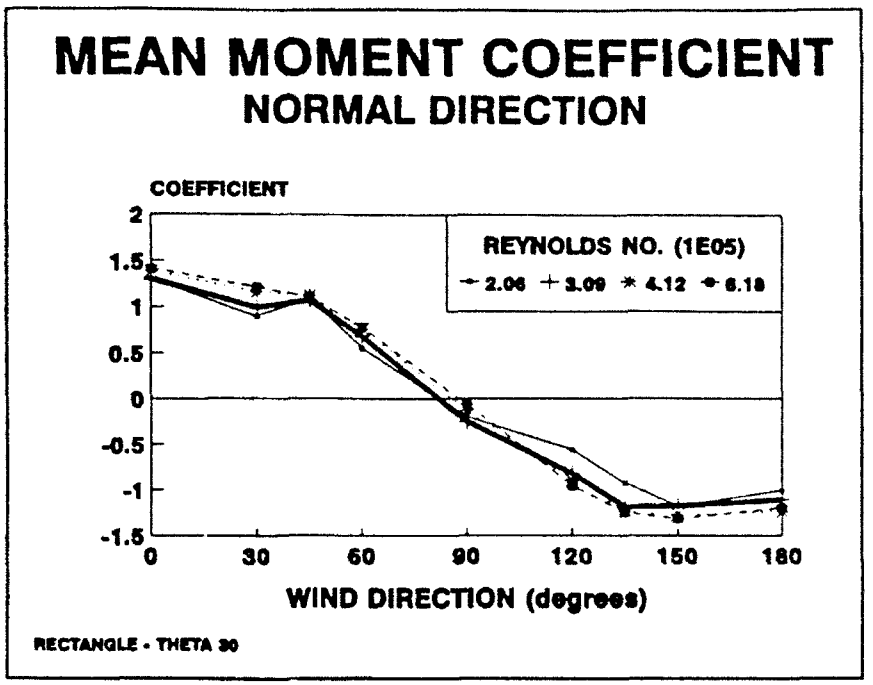

Figure 5. Mean moment coefficient resulting from the normal forces.

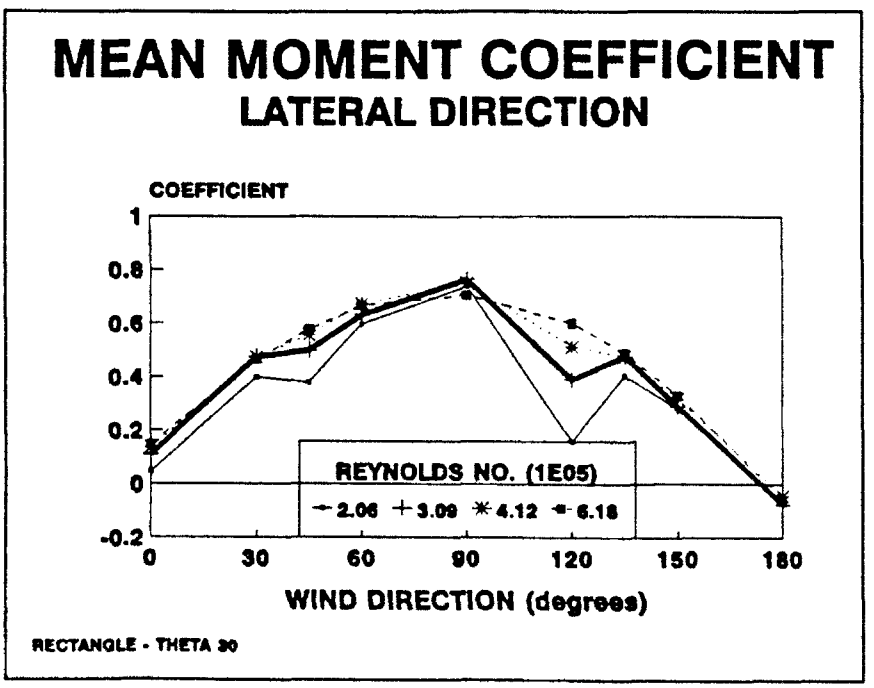

Figure 6. Mean moment coefficients resulting from the lateral forces.

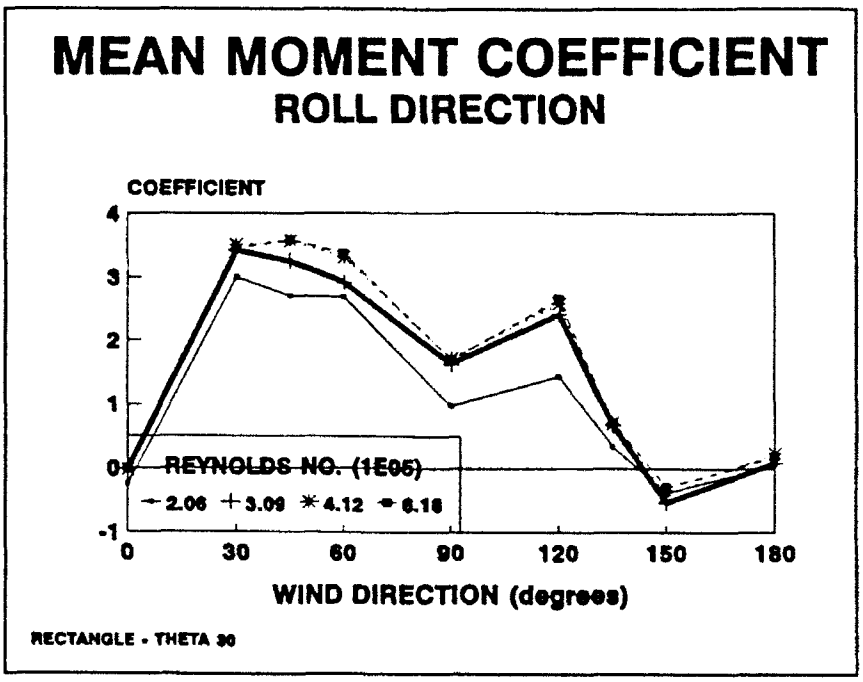

Figure 7. Mean moment coefficient for roll.

where

V is the wind speed
l is the characteristic length chosen to be the object width
ρ is the air density 0.00188388 lbf-s^2/ft^4
μ is the dynamic viscosity of air taken to be $3.6*10^{-7}$ lbf-s/ft^2

Figure 3 shows the mean force coefficient in the normal direction. The change in sign of the coefficient simply reflects the apparent change in direction of the force due to the rotation of the sting. When aligned with the wind (0 and 180 deg) the coefficient is slightly >1 which is in reasonable agreement with the drag coefficients for rectangular plates as reported in most fluid dynamic text books. The force coefficient along the normal direction goes to 0 near 90 deg as expected.

Figure 4 shows the mean force coefficient in the lateral direction. In this case at 0 and 180 deg the coefficient is near 0 as expected and peaks near 90 deg. The peak value of the lateral mean force coefficient is ~0.55 which is about half of the expected value for a flat plate. This is actually self consistent since the frontal area in the lateral direction is slightly less than half of the frontal area in the normal direction upon which all the coefficients are based. Thus if normalized to the actual frontal area, the lateral coefficient at 90 deg would be ~1.1 which is in good agreement with the drag coefficient for rectangular plates.

Figure 5 shows the mean moment coefficient due to the forces acting along the normal direction (note that this is actually a turning moment about the lateral axis). The behavior of the curve is as expected, that is, maxim m overturning moments at 0 and 180 deg and minimum near 90 deg.

Figure 6 shows the mean moment coefficient due to the forces acting along the lateral direction. Note that the peak value is half of what is seen in Figure 5. The primary reason for this is again the difference in actual areas as discussed above.

Figure 7 shows the mean moment coefficient about the vertical axis. The normalizing factor is the same as used in Figures 5 and 6 and consequently has no physical significance. However since the measured moment was dimensionally (inch-pound force) and the normalizing factor was dimensionally (foot-pound force) the actual units of the coefficient are (inch-foot), therefore to nondimensionalize Figure 7 one should divide the coefficient values by 12. The rectangle was mounted on the vertically pointing sting through the center of the base (this was the mounting technique for all the test objects) as shown in Figure 1. This creates a lack of symmetry in the cross-sectional area about the sting. This lack of symmetry causes a moment about the vertical axis and is a maximum when the tilted rectangle is at an azimuth of 90 deg. Typically however the tilted objects exhibit maximum coefficient values at azimuths significantly different from 90 deg. This is probably due to a stagnation zone created by flow over the top of the test object.

4.2 POWER SPECTRA

Before beginning the discussion of power spectra it will be helpful to discuss the power spectra units. Recall from Section 3.0 that the actual forces and moments were normalized to yield unitless force and moment coefficients. The power spectra presented are the power spectra of the coefficients, thus the power spectra has units of inverse hertz (Hz^{-1}). When integrated over a spectral range the power spectrum will yield a unitless number. To calculate the magnitude of the unsteady force caused by vortex shedding integrate the power spectrum over the spectral region which contains the vortex shedding, then multiply the square root of the integral by the normalizing factor. For example, in Figure 8 the shedding region for the 120 ft/s tunnel velocity extends from 25.6 Hz to 33.2 Hz. In this region the power spectral density (PSD) integral increases from 0.000785 to 0.003300. Thus the net increase in the integral over the region is 0.00252, the square root of which is 0.05. Therefore the standard deviation of the unsteady force in the lateral direction, F'_l, due to vortex shedding in this spectral region is,

$$F'_l = \left(\tfrac{1}{2} \rho V^2 A \right) * 0.05$$

Because of the error in processing the data, discussed in Section 3.0, the units of the power spectra of the moment about the vertical axis are actually inch per square foot per hertz ($[in/ft^2]/Hz$) instead of inverse hertz. To correct the error divide the indicated values of the power spectra (or the power spectra integral) by 144 to obtain the correct value for a unit of Hz^{-1}.

The force and moment power spectra were computed using the full 2048 points. No attempt to average the spectra through segmenting or overlapping was made. The resulting PSD had frequency intervals of 0.361 Hz from 0 Hz to the Nyquist frequency of 370 Hz. The vortex shedding frequencies were expected to be below 50 Hz. Aliasing would only be a problem if frequencies were above 370 Hz. A potential for signal contamination exists if the natural vibrational frequency of the test object is near the shedding frequencies. Table 1 shows the natural frequencies for the test objects. The PSD plots, in general, are only displayed out to 50 Hz. Once plotted the PSD plots were subjectively categorized based on the quality of the shedding signature. Ideally, the shedding signature would be a single frequency spike, the frequency of which would be a linear function of the tunnel wind speed. Based on this ideal, four categories, A through D, were created which were called very good shed, good shed, poor shed, and no shed respectively. The very good shed data have a clearly identifiable shedding frequency (or in the case of multiple frequencies, a clearly identifiable spectrum) with little or no noise present. The good shed data are identifiable but the noise level is such that extent of the shedding spectrum is uncertain. The poor shed data are so contaminated with noise that shedding is only barely identifiable. The no shed data give the appearance of noise (although not necessarily white noise). The following paragraphs will provide specific

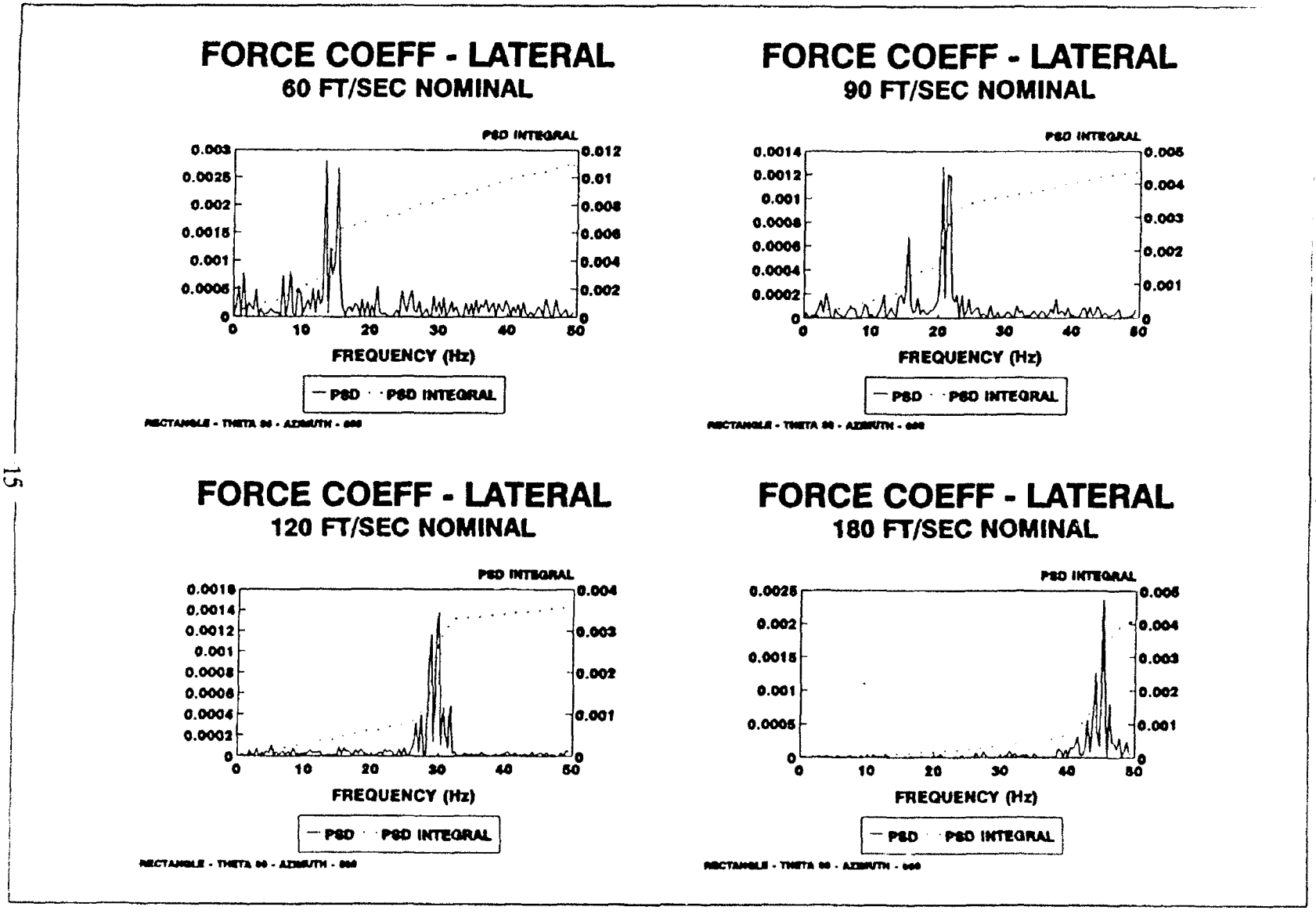

Figure 8. Category A (very good) force coefficient power spectra in the lateral direction.

examples of these categories. Table 2 presents a summary of the data, grouped into these categories, based on the test object and orientation.

Figure 8 shows the lateral force coefficient power spectra for the very good shed data for the rectangle at an orientation of 0 deg. The shedding frequency, although not a single frequency, is clearly identifiable. A quite linear relation can be seen between the principle frequency and the wind speed. Since the force and moment coefficients are different linear combinations of the two force measurements (recall Section 3.0) it is not surprising that the lateral moment coefficient also shows a very good shed signature. This is shown in Figure 9. Figure 9 shows that the data are nearly linear with wind speed and there is minimal noise.

It is interesting to point out a difference that exists between the force and moment coefficient spectra plots at 60 ft/s. The force coefficient spectrum shows two distinct spikes at 13.369 Hz and 15.176 Hz of ~0.0027 magnitude. At the same frequencies the moment coefficient spectrum also shows two spikes of differing amplitudes, the larger is 0.0045 and the smaller is 0.0015. There are two possible explanations for why similar forces at different frequencies would give rise to differing moments. One explanation is that the difference results from a fundamental difference in the origin of the forces. For example at one frequency the force might be due to a tunnel vibration transmitted to the sting via the mounting hardware while at the other frequency the force is due to the vortex shedding of the test object. Another possible explanation is that different points on the test object shed at different frequencies. Shedding frequency variations have been noted and discussed by Ayoub and Karamcheti (Ref. 4), Gerich and Ecklemann (Ref. 5), Eisenlohr and Eckelmann (Ref. 6), Williamson (Ref. 7), König, Eisenlohr, and Eckelmann (Ref. 8), and Stäger and Eckelmann (Ref. 9). Of the studies mentioned only Ayoub and Karamcheti (Ref. 4) noted similar Reynolds numbers, that is, 10^5 -10^6. Although Ayoub and Karamcheti collected data at similar Reynolds numbers their test configuration was sufficiently different to eliminate direct comparisons. Further analysis of the differences in frequency spikes between forces and moments could help discriminate between noise and shedding signatures. An attempt was made to use transfer function and coherency function analysis for the purpose of separating noise and signal. The results were inconclusive due to the small size (2048 points) of the data sample.

Because of the inclination of the test object it seems reasonable to expect that forces acting on the lateral faces would induce a moment about the vertical axis. Figure 10 shows the PSD of the moment coefficient about the vertical axis (roll). A comparison of Figure 10 with Figures 8 and 9 clearly indicates that the shedding can indeed be seen in the axial roll data. In this particular case however the roll data are noisy and viewed separately would be classified as poor shed data.

Table 2. Wind tunnel data summary.

SHAPE	DECLINATION (degrees)	DIMENSIONS LxWxH (in)	WEIGHT (grams)	AZIMUTHAL ANGLE (degrees)								
				0	30	45	60	90	120	135	150	180
CYLINDER	0	8.1 x 8.1 x 10.0	1130.5	D								
CYLINDER	0	8.1 x 8.1 x 8.0	1029.5	D		D		D				
CYLINDER	30	8.99 x 8.08 x 8.99	898.1	C	D	D	D	D	D	D	D	C
CYLINDER	45	11.12 x 8.12 x 8.46	897.0	C	D	D	D	D	D	D	D	A
OCTAGON	0	8.0 x 8.0 x 10.0	1659.3	C	C	C	D	C				
HEXAGON	0	8.0 x 8.0 x 10.0	1615.0	B	C	C	D	D				
CUBE	0	7.64 x 7.9 x 6.03	735.5	A	D	D	D	A				
CUBE	0	7.66 x 7.91 x 7.91	873.8	A	D	D	D					
CUBE	0	7.62 x 7.88 x 9.56	1009.5	A	D	D						
CUBE	30	9.0 x 7.7 x 8.5	951.1	C	B	D	D	A	B	B	B	C
CUBE	45	11.1 x 7.88 x 8.31	1029.5	D	B	D	D	A	C	B	A	D
R'ND CUBE	0	8.0 x 8.0 x 10.0	1700.0	D	D	D	D	D				
R'ND CUBE	30	9.0 x 8.0 x 8.9	1575.4	D	C	B	D	D	B	A	B	D
RECTANG	0	3.9 x 7.9 x 7.76	691.1	A	D	D	D	D				
RECTANG	0	4.06 x 8.0 x 4.0	925.9	A	D	D	D	D				
RECTANG	30	9.13 x 4.06 x 8.69	755.8	C	C	B	D	A	B	D	D	D
RECTANG	30	4.54 x 7.96 x 4.46	750.9	A	A	D	D	D	D	C	B	D
RECTANG	45	11.4 x 3.92 x 8.5	695.0	D	B	B	B	A	A	C	D	D

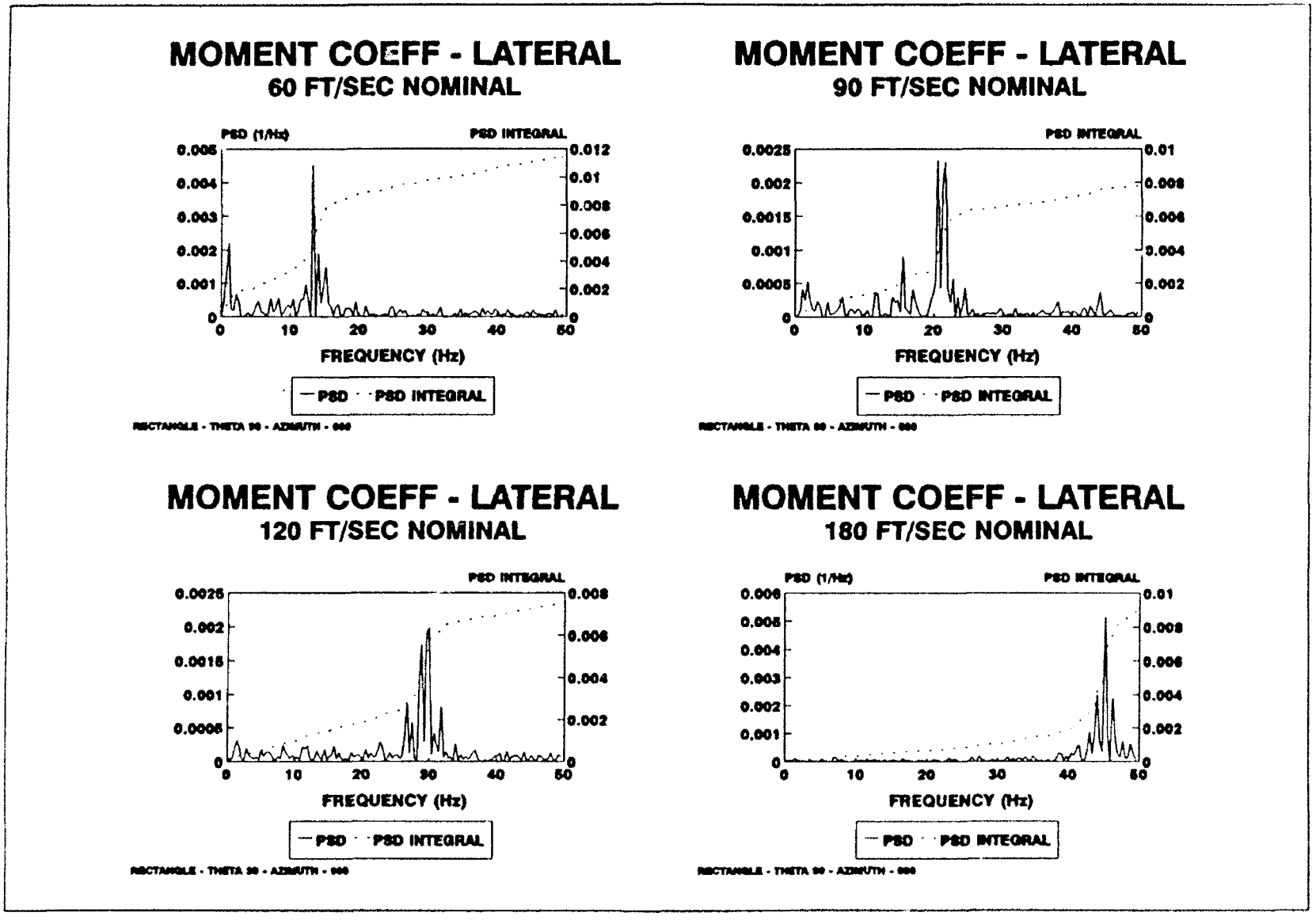

Figure 9. Category A (very good) moment coefficient power spectra caused by lateral forces.

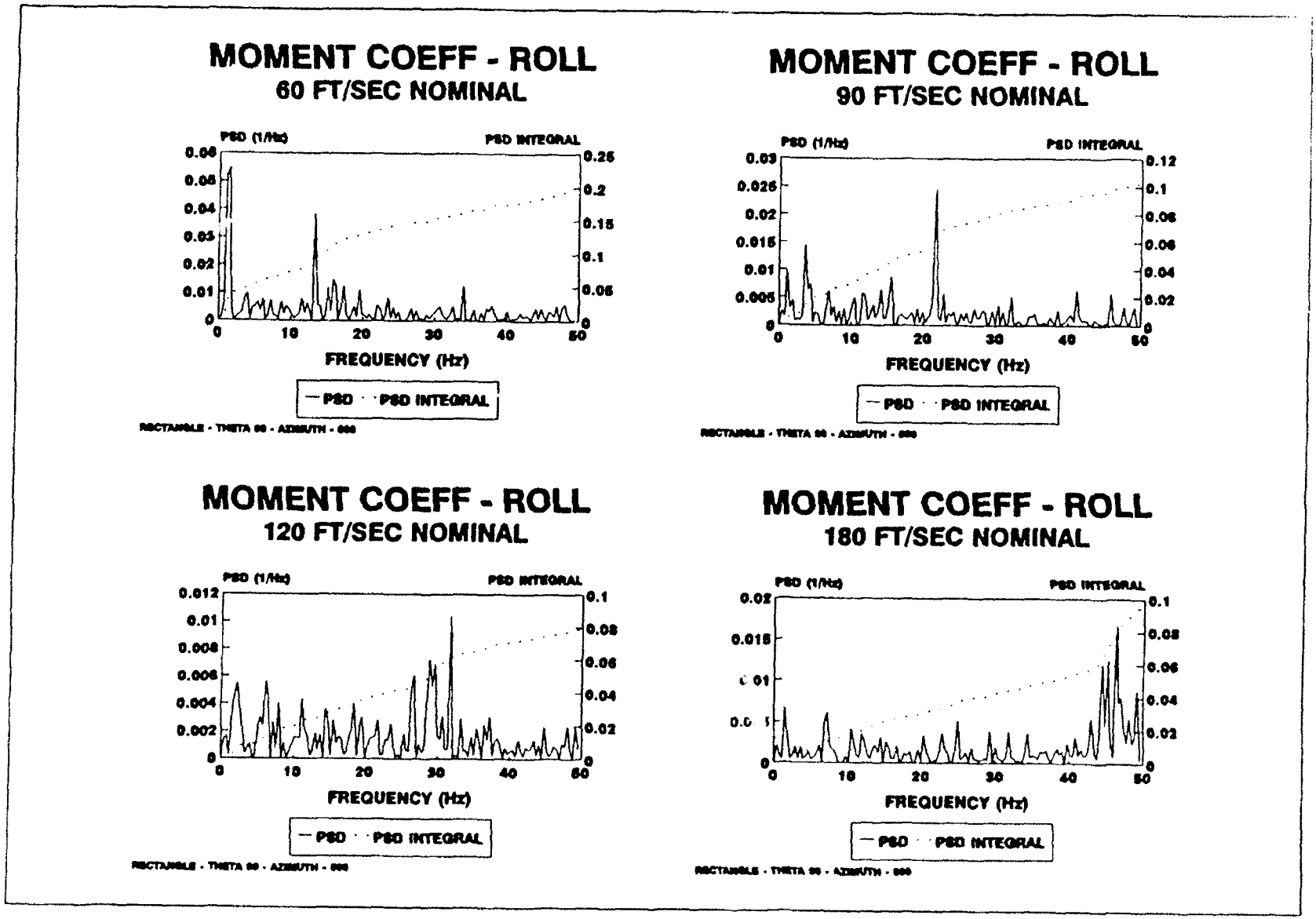

Figure 10. Category A (very good) roll moment coefficient power spectra.

An example of good shed data can be seen in Figures 11 through 13, which is the rectangle at an azimuth of 150 deg. By comparing the PSDs of the lateral force, lateralmoment, and roll coefficients one can readily determine that shedding is occurring, however the noise levels appear higher then in Figures 8 through 10. Again, comparing the PSD spikes suggests that differences in the points of application exist and that perhaps these differences can be exploited to discriminate between signal due to vortex shedding and noise caused by tunnel resonances.

Figures 14 through 18 provide an example of poor shed data for the rectangle at an azimuth of 135 deg. These figures show an increase in the region 35 to 40 Hz at 180 ft/s. At 120 ft/s the figures show some activity in the 20 to 25 Hz band. At 90 ft/s there seems to be signal in the 15 to 20 Hz band. At 60 ft/s the increased signal levels seem to be locked around 15 Hz. These regions of increased signal correspond well to the speeds but are exceptionally noisy.

Figures 14 through 18 tend to display a curious phenomena often observed in the data: that is, a frequency spike near 15 Hz. The origin of this spike is not known. The natural frequency of the test objects were measured as described by Jumper, et.al. (Ref. 1) and are shown in Table 2. As can be seen, neither the rectangle cited in this example nor any of the other test objects exhibited natural resonances near 15 Hz. There are several possible explanations. It is possible that a tunnel vibration at 15 Hz was coupled to the sting. However Jumper, et.al. (Ref. 1) claimed that this was evaluated and that tunnel vibrations were several orders of magnitude below the shedding signature. Another possibility is that the 15 Hz is an acoustic wave that is set up in the tunnel. Finally it is possible that it is a lock-on phenomenon. A good review of lock-on phenomena has been done by Griffin and Hall (Ref. 2) and it is possible that a small vibration (acoustic or structural) could significantly affect the shedding frequencies. No definitive answer to this often observed spike was possible during this analysis effort.

Figures 19 through 23 show the rectangle at an azimuth of 45 deg, a case where no shedding signature could be discerned. In these instances the plots are generally quite noisy. Notice that the PSD spike near 15 Hz is present in much of these data.

4.3 STROUHAL NUMBER

Only the very good shedding data, as indicated in Table 2 are presented in this analysis. The Strouhal number is calculated as

$$S = \frac{fd}{V}$$

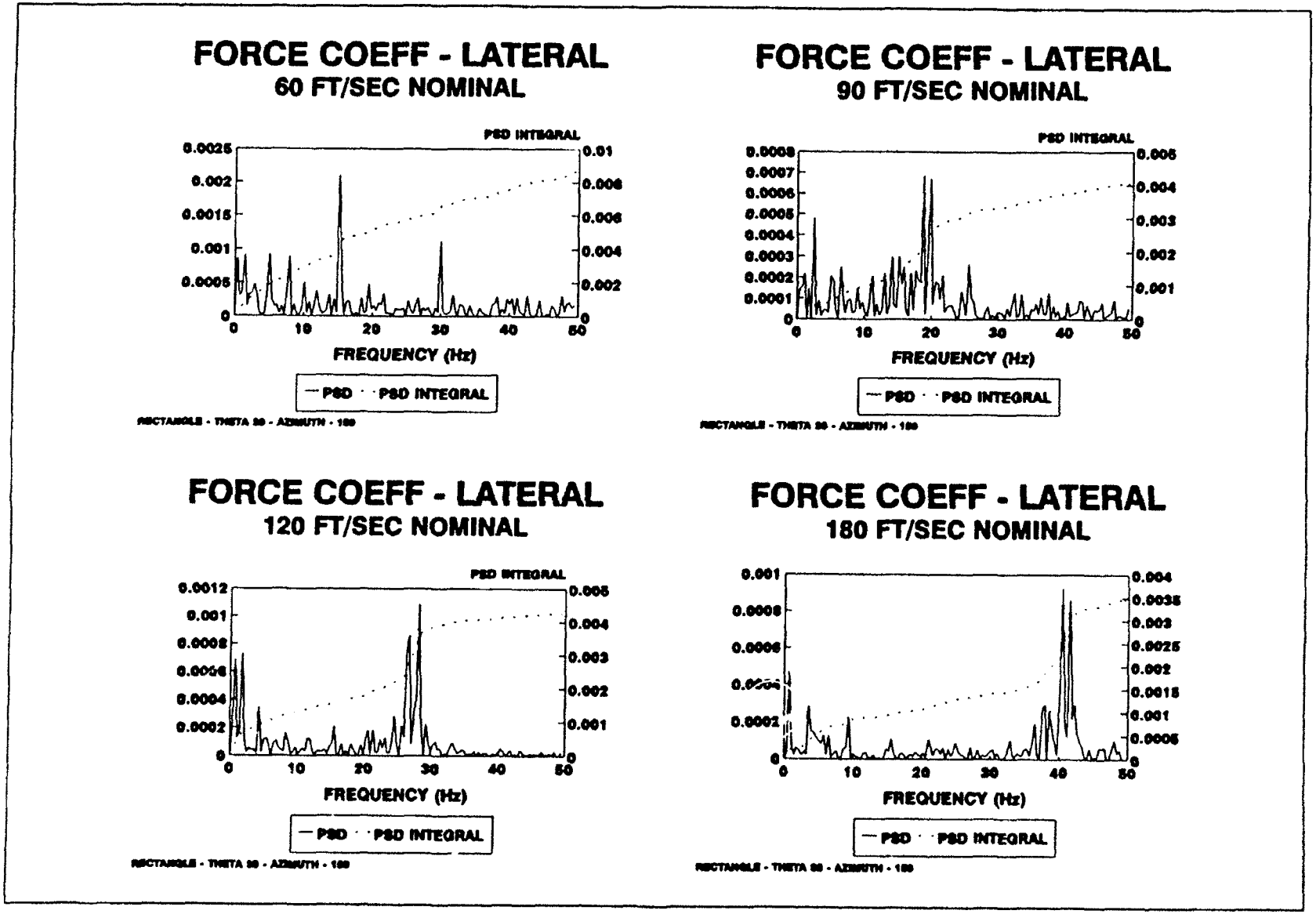

Figure 11. Category B (good) force coefficient power spectra in the lateral direction.

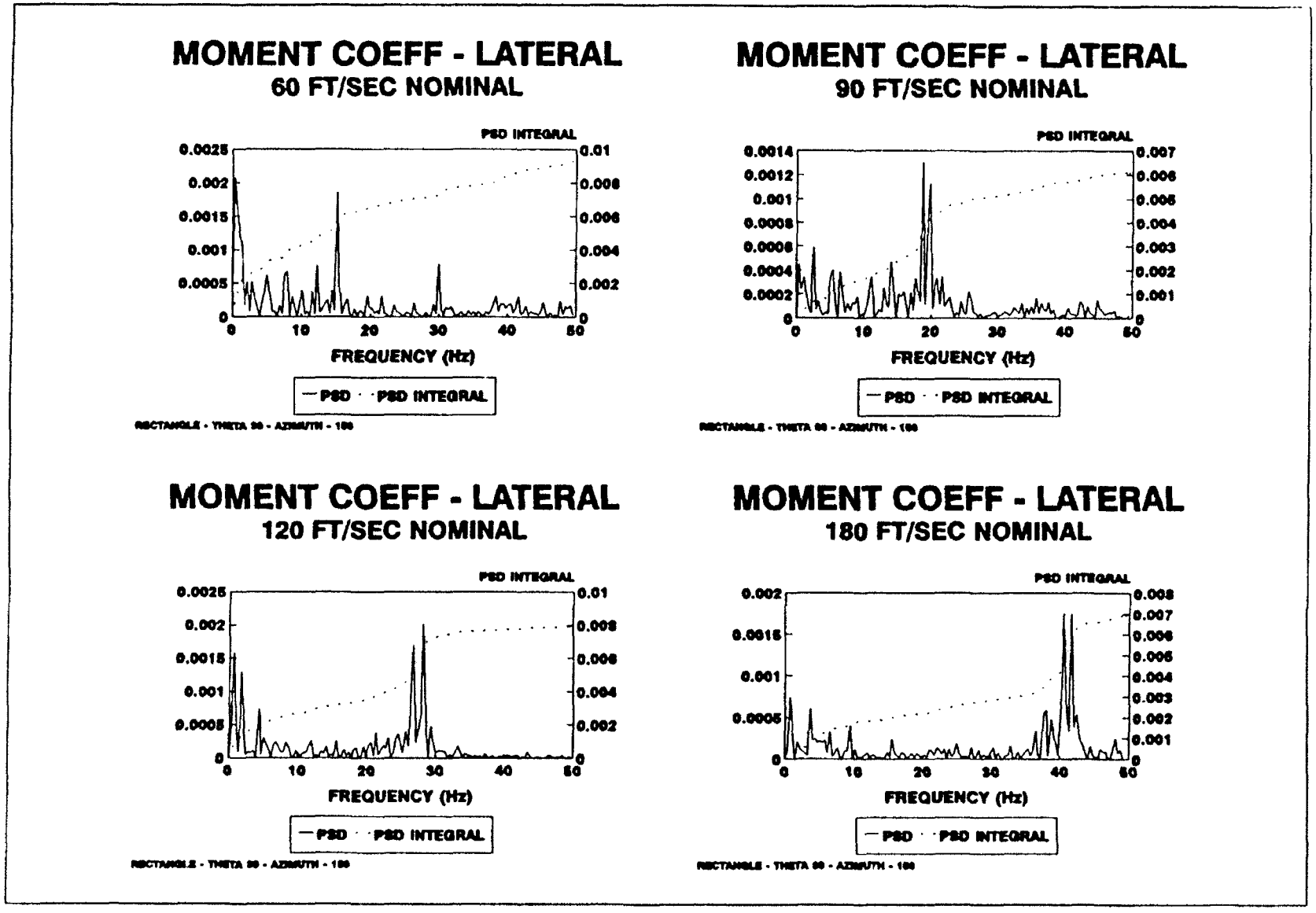

Figure 12. Category B (good) moment coefficient power spectra caused by lateral forces.

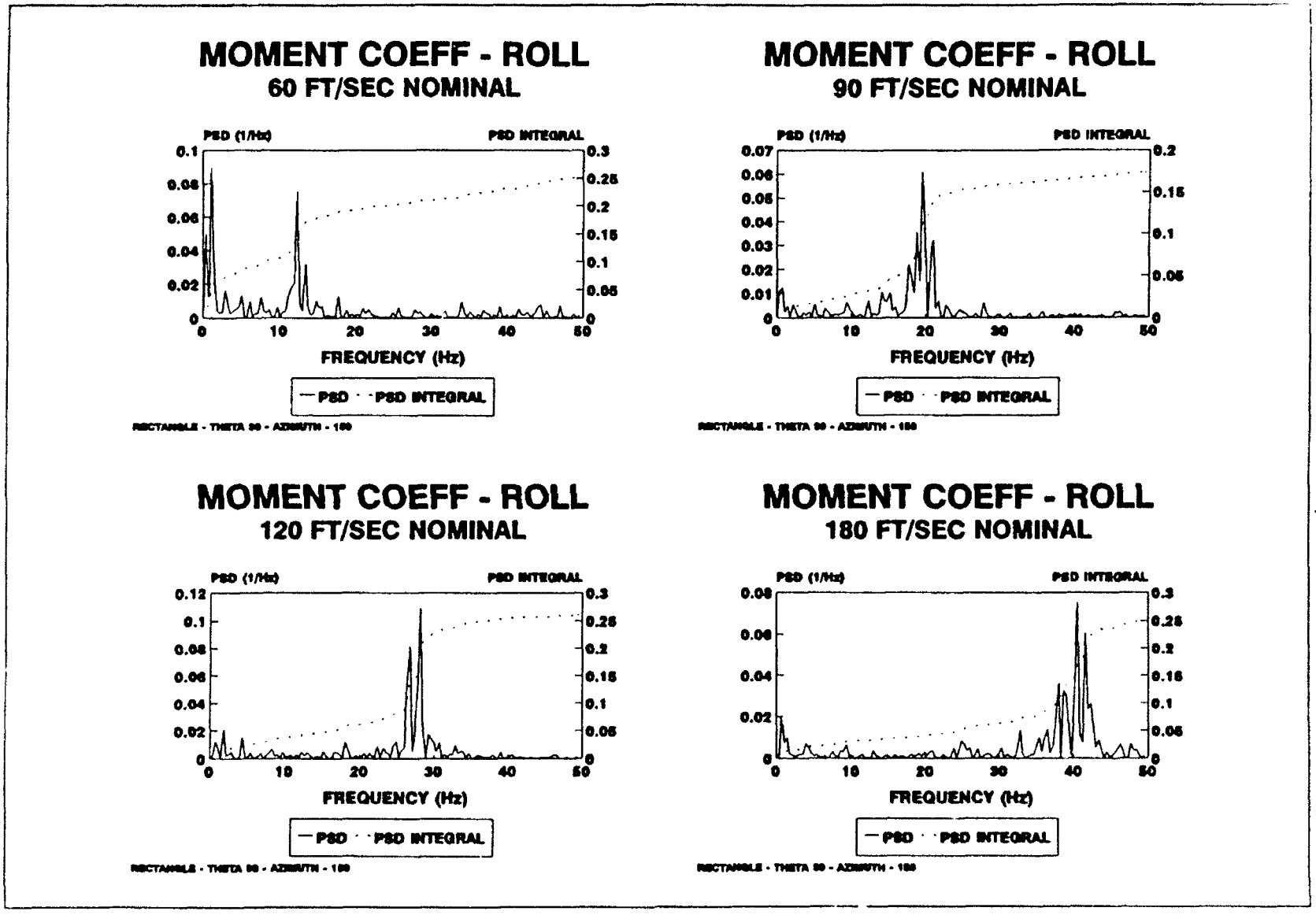

Figure 13. Category B (good) roll moment coefficient power spectra.

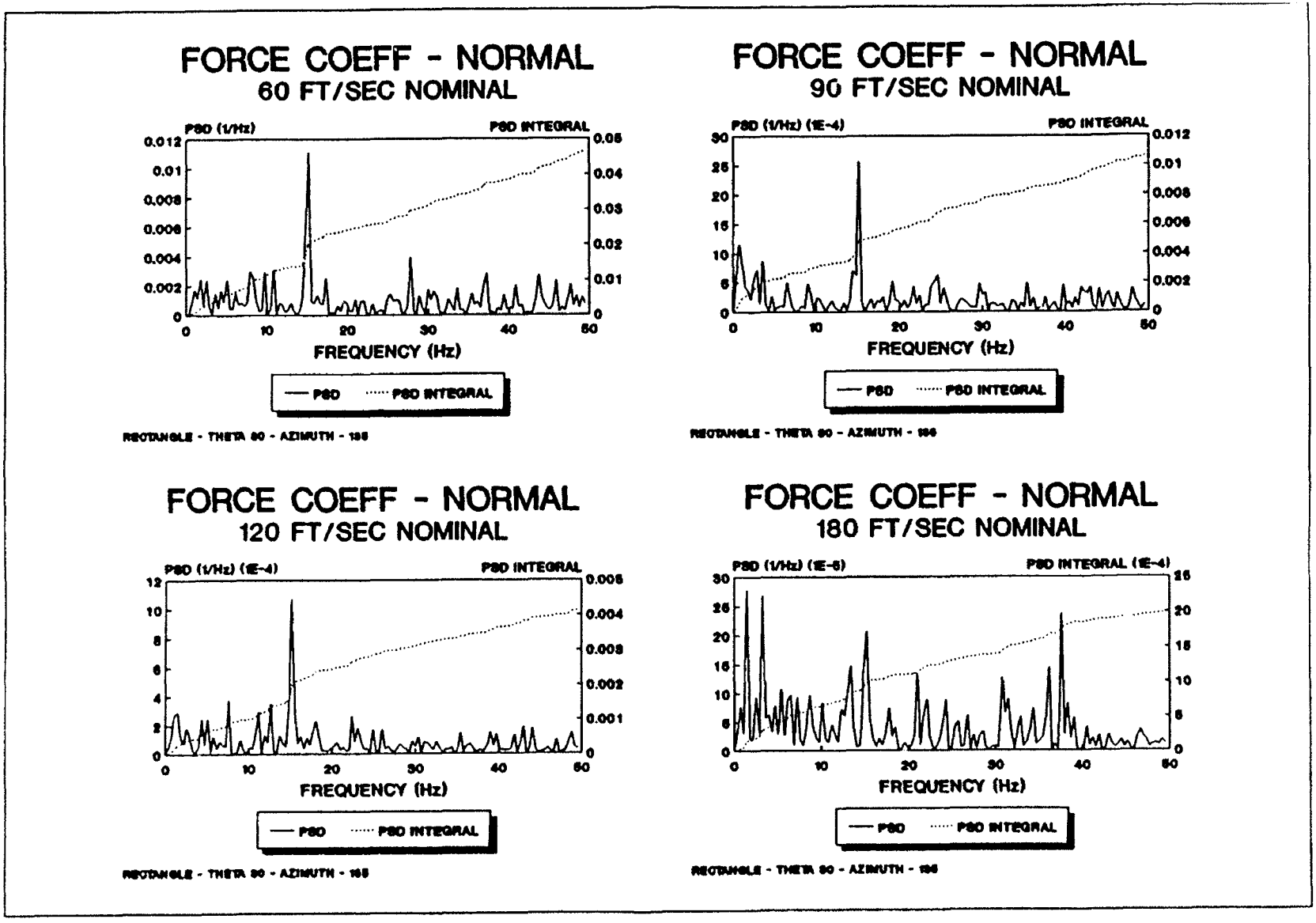

Figure 14. Category C (poor) normal force coefficient power spectra.

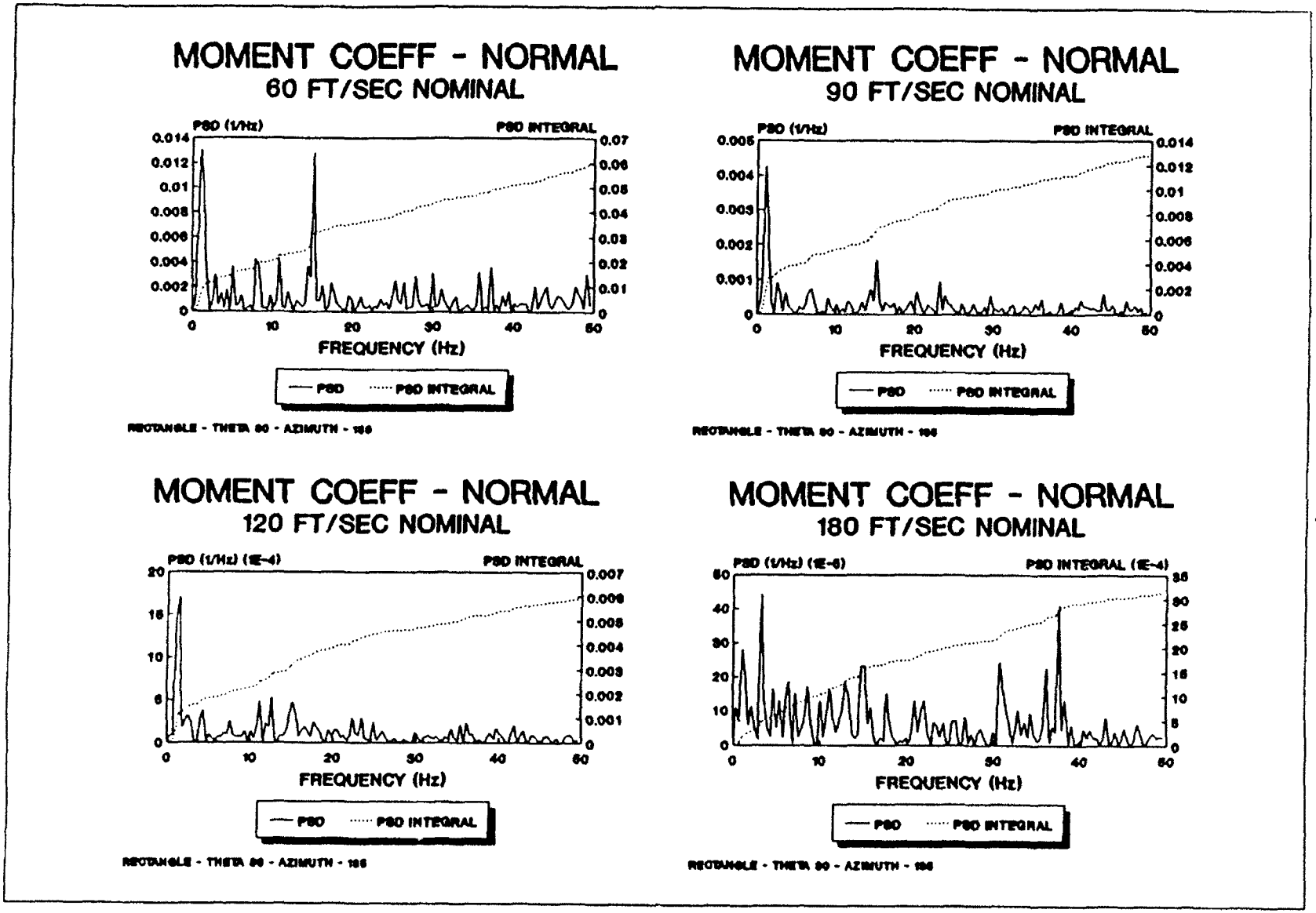

Figure 15. Category C (poor) normal moment coefficient spectra.

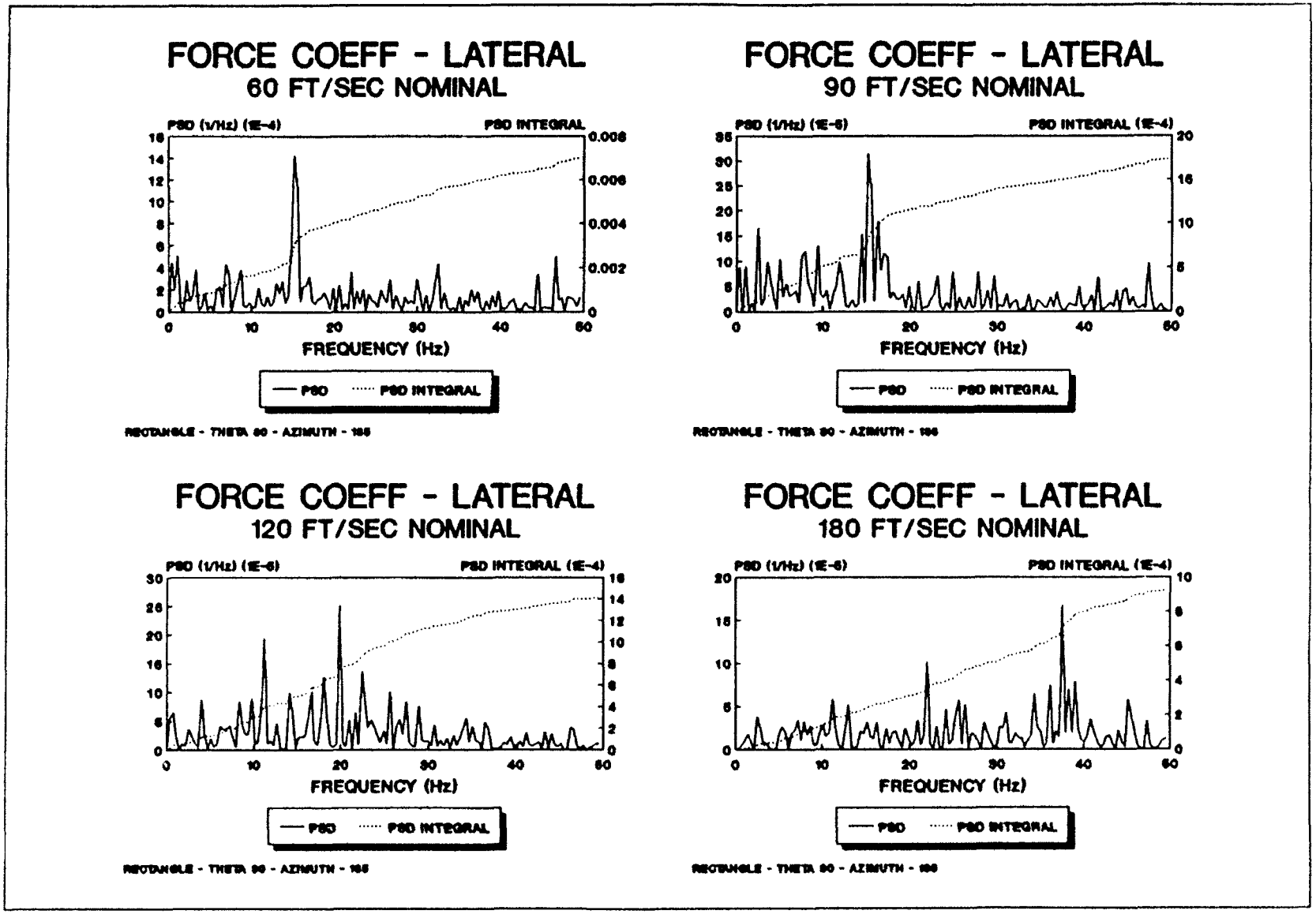

Figure 16. Category C (poor) lateral force coefficient spectra.

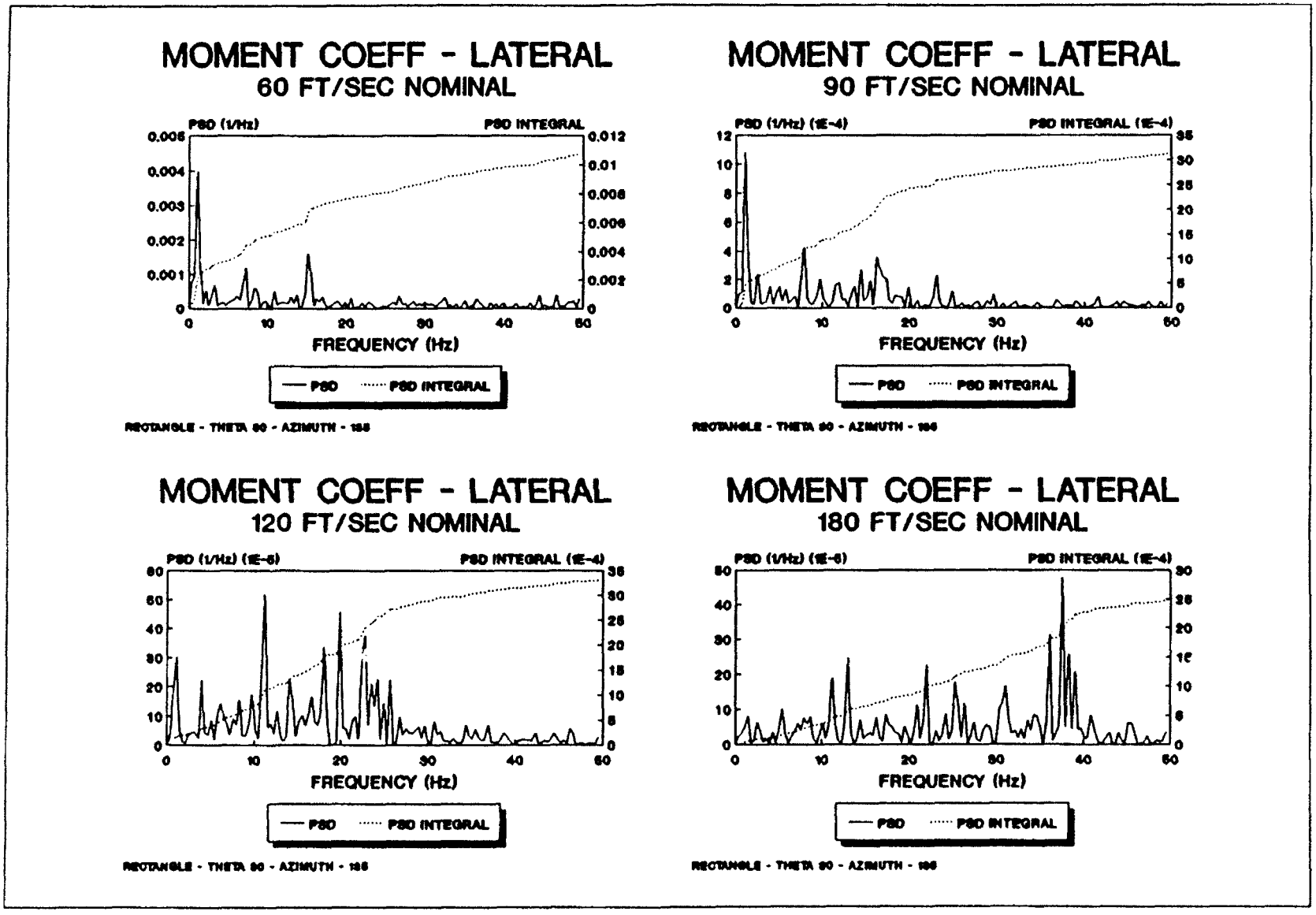

Figure 17. Category C (poor) lateral moment coefficient spectra.

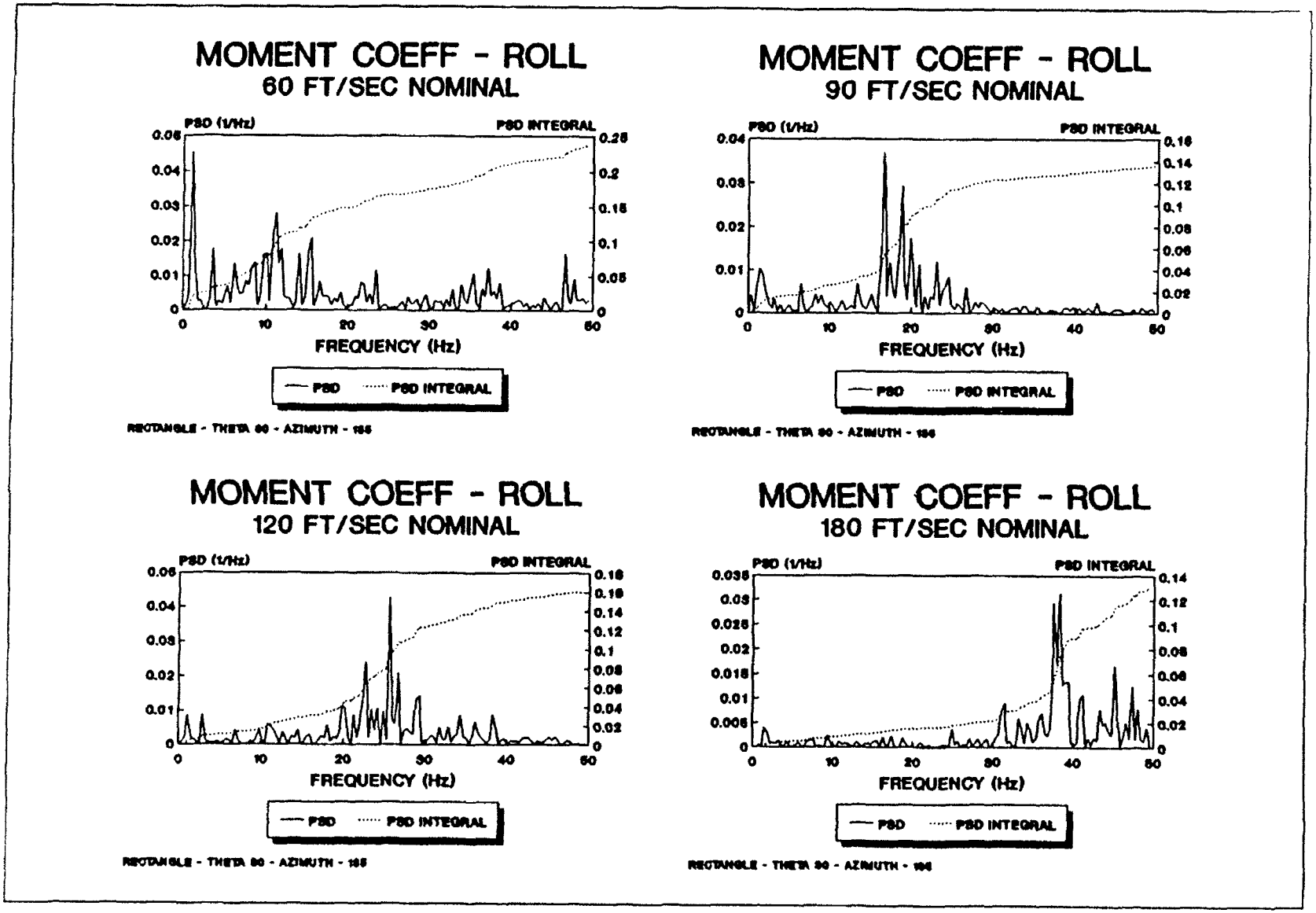

Figure 18. Category C (poor) roll moment coefficient spectra.

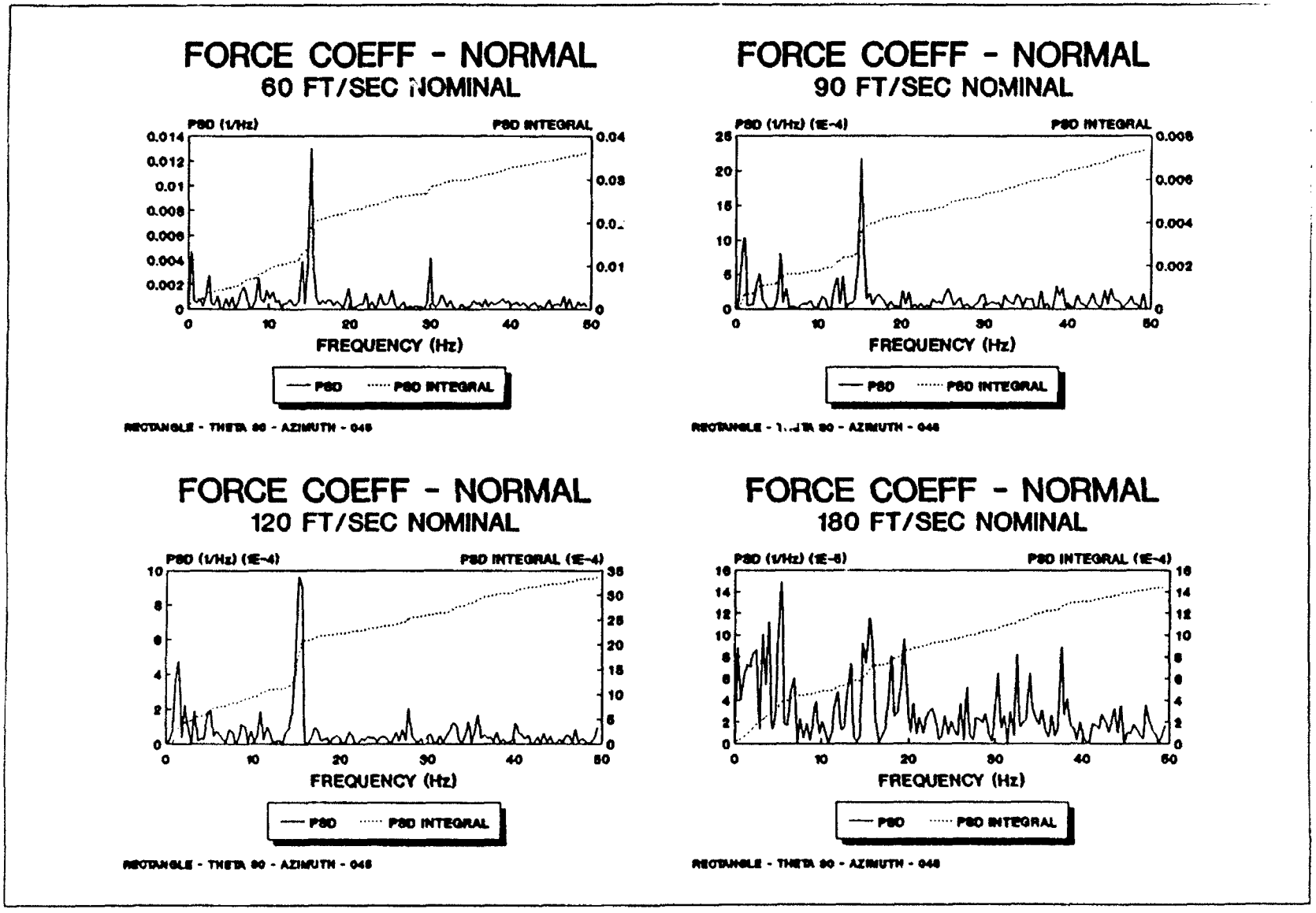

19. Category D (no shed) normal force coefficient spectra.

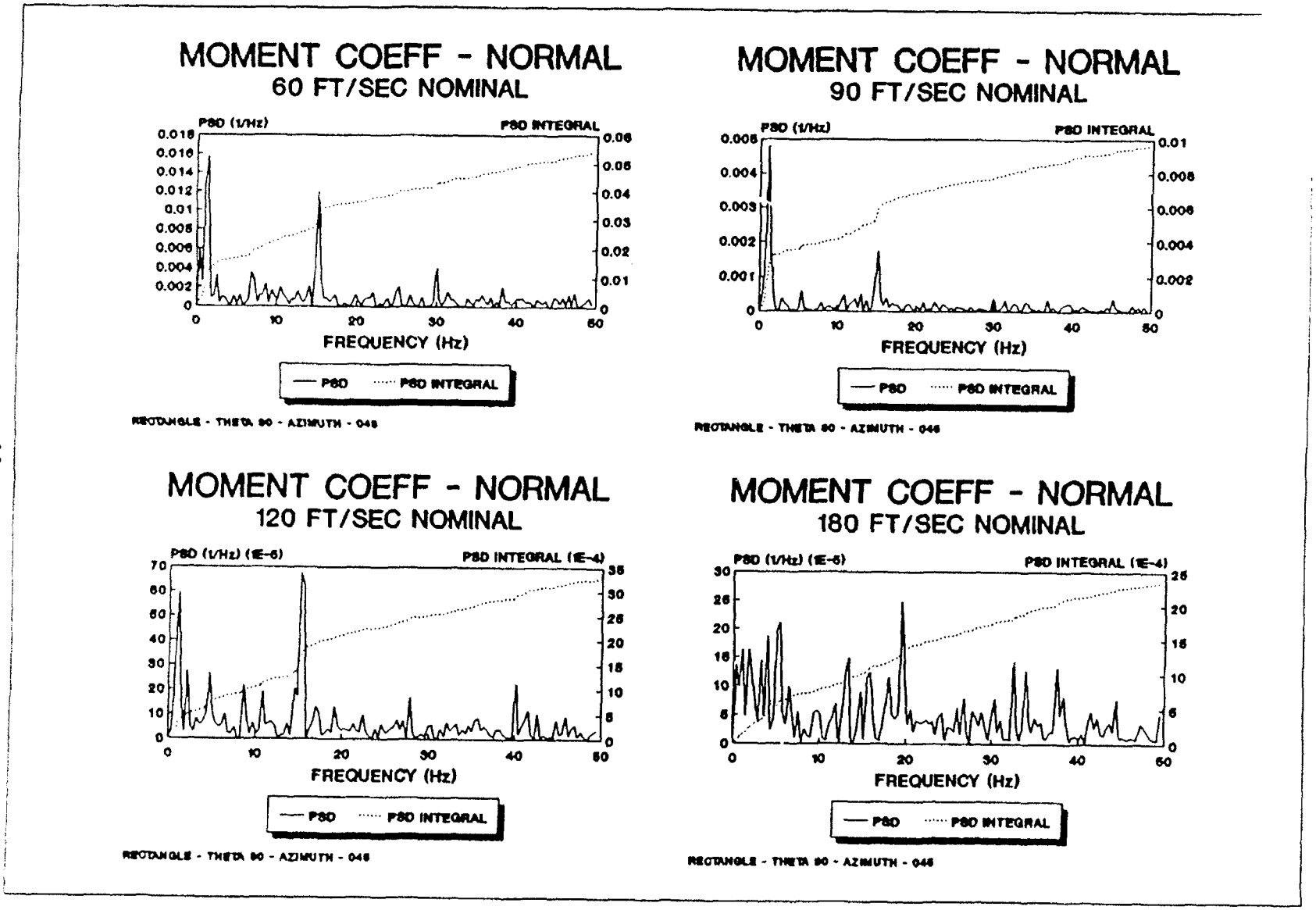

Figure 20. Category D (no shed) normal moment coefficient spectra.

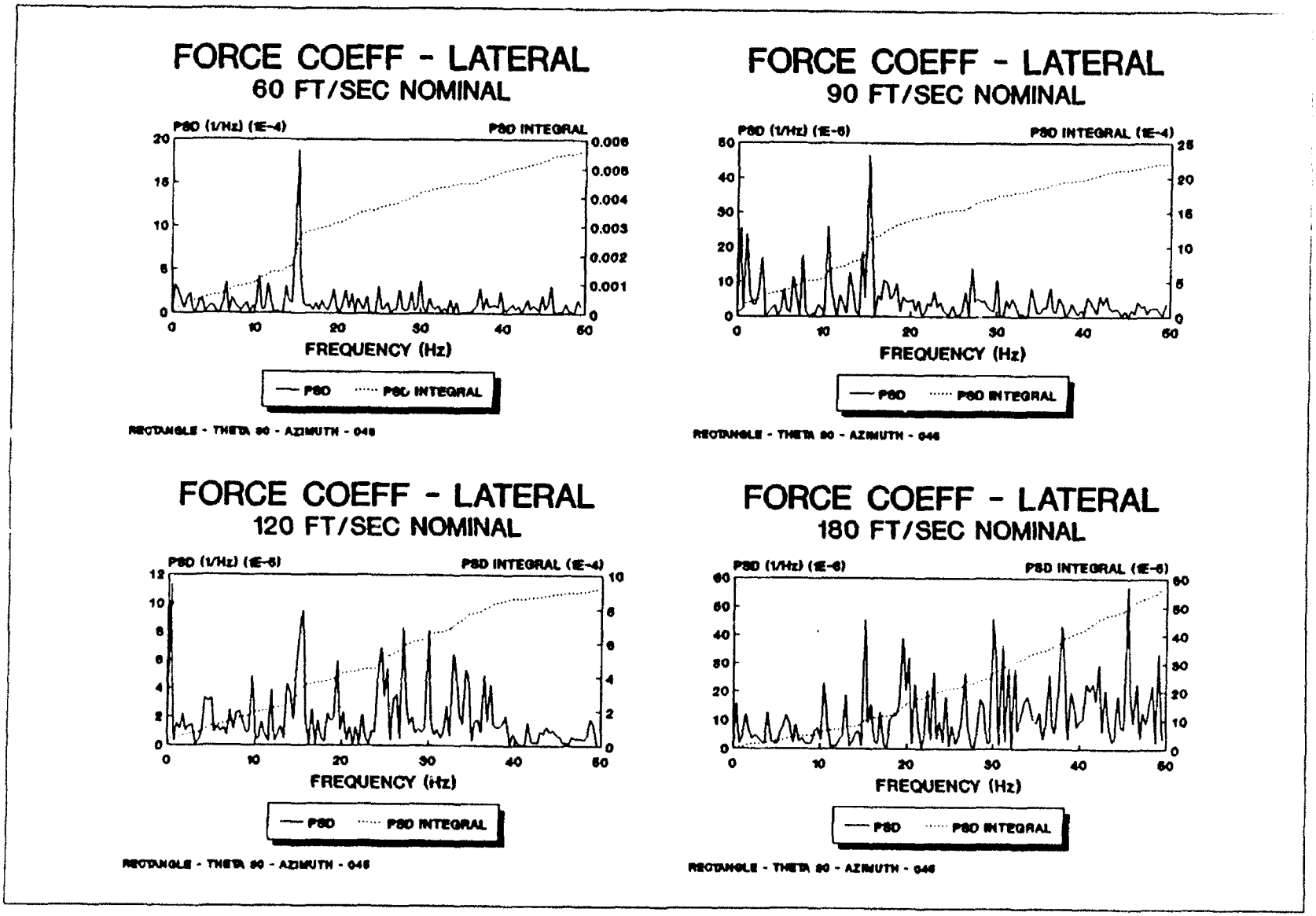

Figure 21. Category D (no shed) lateral force coefficient spectra.

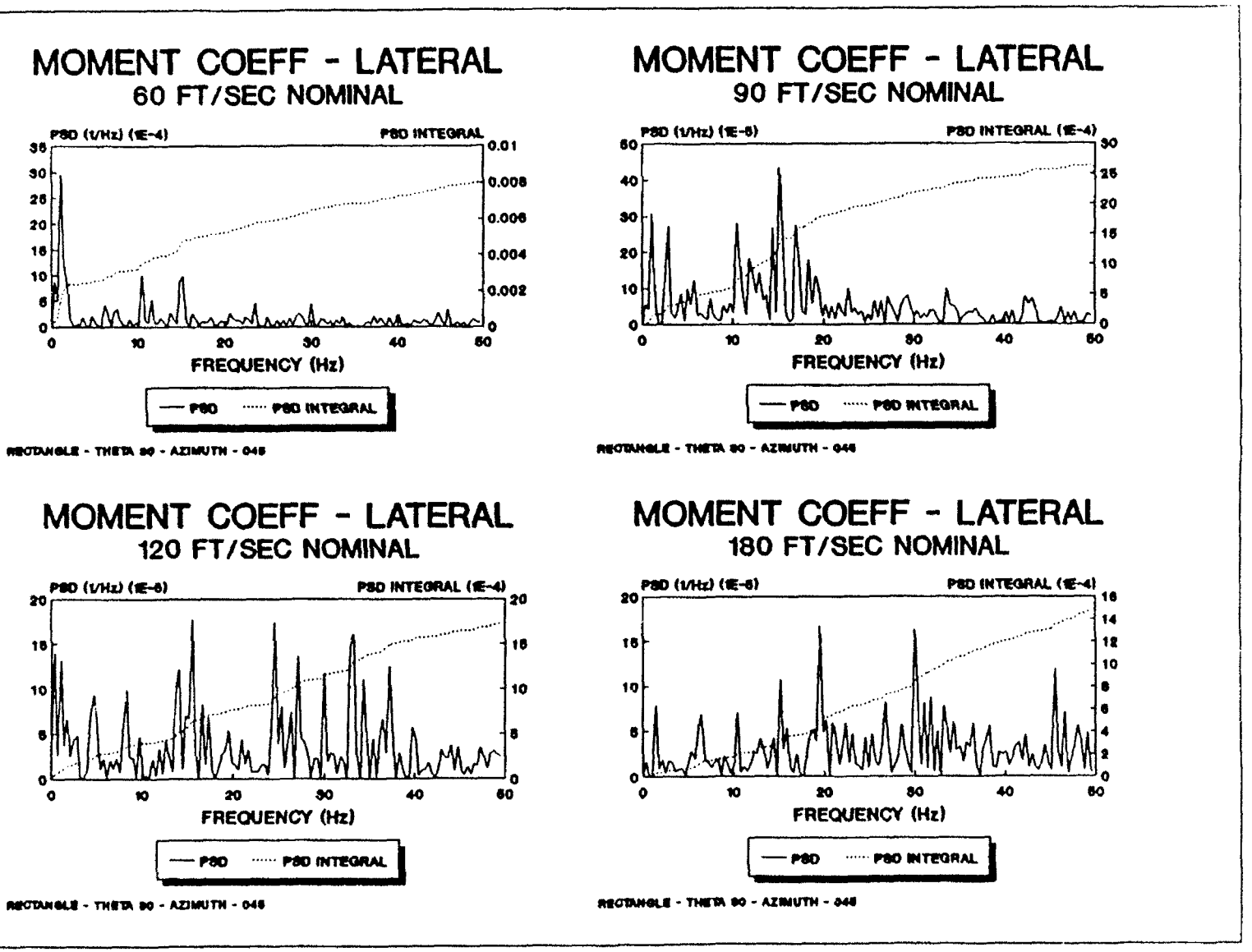

Figure 22. Category D (no shed) lateral moment coefficient spectra.

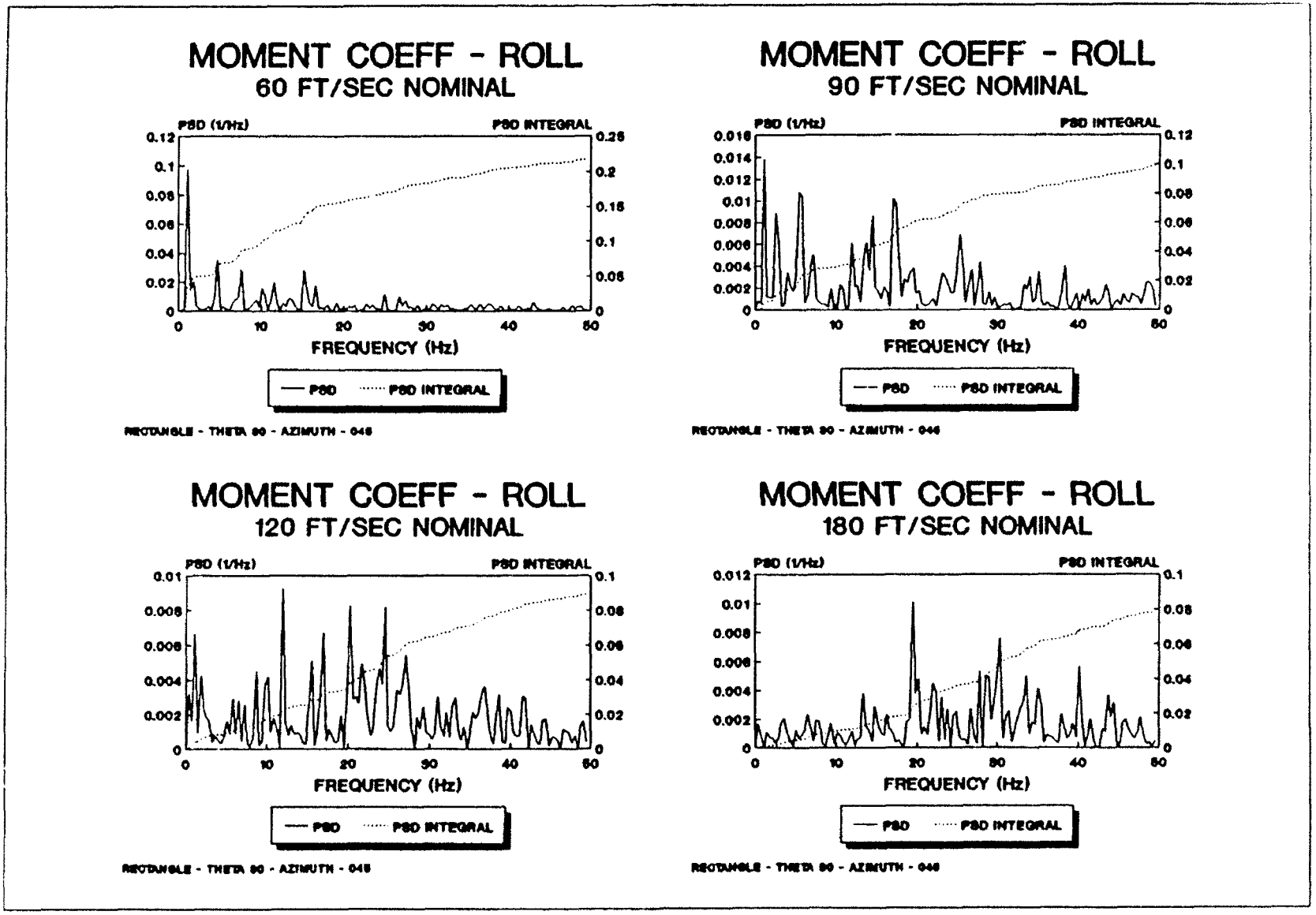

Figure 23. Category D (no shed) roll moment coefficient spectra.

where

f = shedding frequency
d = characteristic length of object
V = wind speed.

The characteristic length chosen is the width based on the cross-section that the test object presents to the wind. For the case of a tilted test object or the case where multiple faces may be presented to the wind flow, the cross-sectional width is taken as the shortest projected dimension across the object as shown in Figure 24.

Ideally, the spectral vortex shedding signature would be a delta function, the exact frequency of which is proportional to the wind speed. However, in most instances the observed shedding occurred over a spectrum as shown in Figures 8 through 10. In these cases several shedding frequency peaks were used to provide a range of Strouhal numbers. Figure 25 shows the resulting Strouhal number as a function of tunnel wind speed, test object, and orientation. In general, the Strouhal number displays very little dependency upon the tunnel wind speed. Thus it appears that the above Strouhal number equation can be extended to cover spectral peaks for cases where shedding occurs over a spectral region instead of a single frequency. Figure 25 also indicates that the lowest Strouhal numbers tend to occur for objects oriented with a nonzero declination and an azimuth of 90 deg. A study of Strouhal number as a function of orientation was not undertaken during this study due to the small data set and the lack of resources.

Figure 26 is a summary chart which shows the Strouhal number as a function of the drag coefficient. Each point in Figure 26 represents the average value over the four wind speeds for a given shape, declination angle, and azimuthal angle. The data of Figure 26 are displayed in tabular form in Table 3. Table 3 is useful for identifying the shape and orientation corresponding to a particular data point in Figure 2[illegible] For the Strouhal number average, when several shedding frequency peaks were used to provide a range of Strouhal numbers, all the numbers were used in computing the average. For the drag coefficient the actual area presented to the tunnel flow was used instead of the constant area discussed in Section 3.0 and used to computing the mean force coefficient plots shown earlier. Figure 26 suggests an inverse relationship between Strouhal number and drag coefficient. Hoerner* showed a similar relationship for Reynolds numbers greater than 1000. The empirical relationship given by Hoerner was

$$S = \frac{0.21}{C_D^{3/4}}$$

The data presented in Figure 26 are 60 to 70 percent of the values predicted by Hoerner's equation.

*Hoerner, S. F., Fluid-Dynamic Drag, published by the author, 1958.

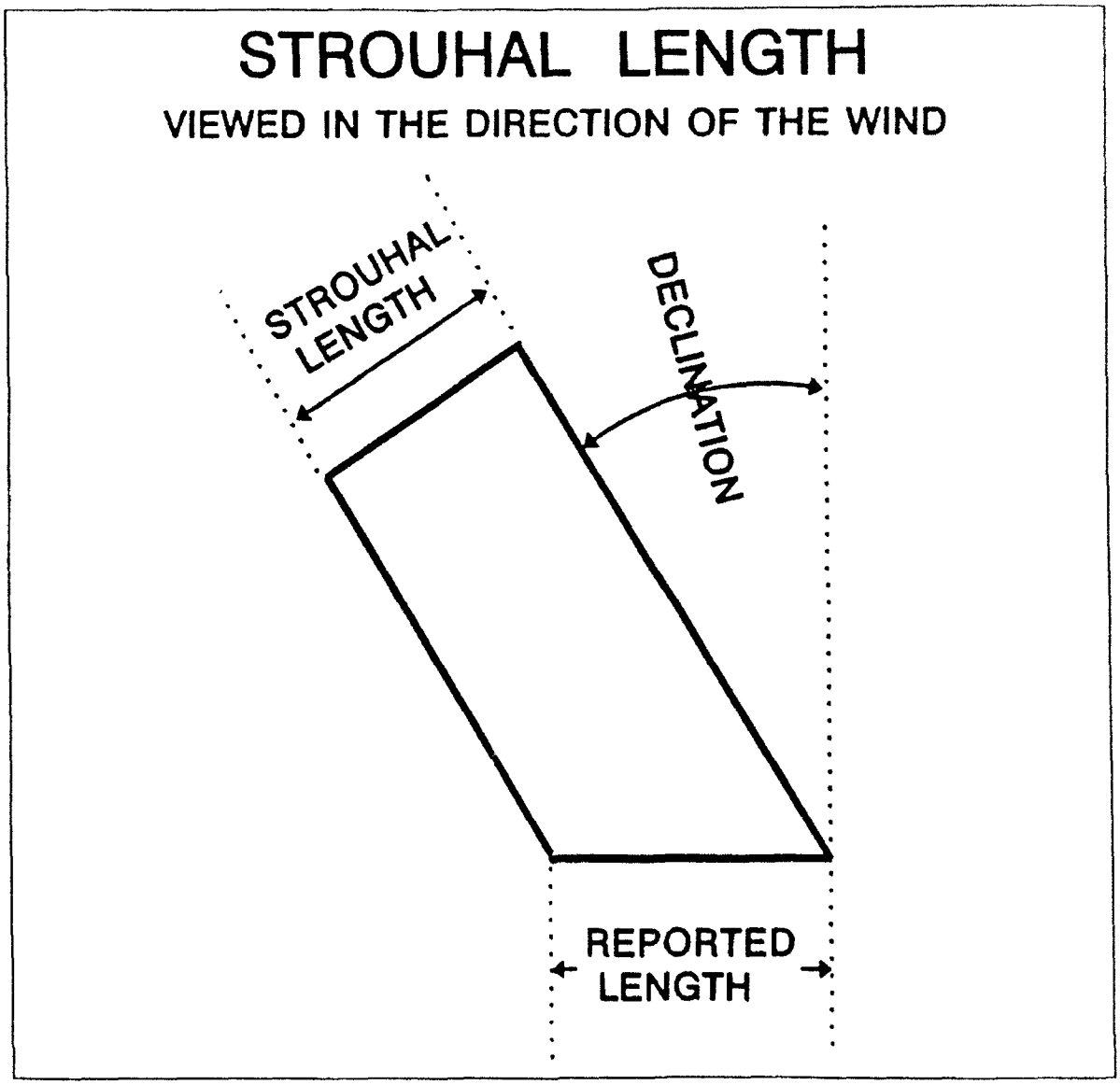

Figure 24. The length used in Strouhal calculations is not necessarily the length reported in Tables 1 and 2.

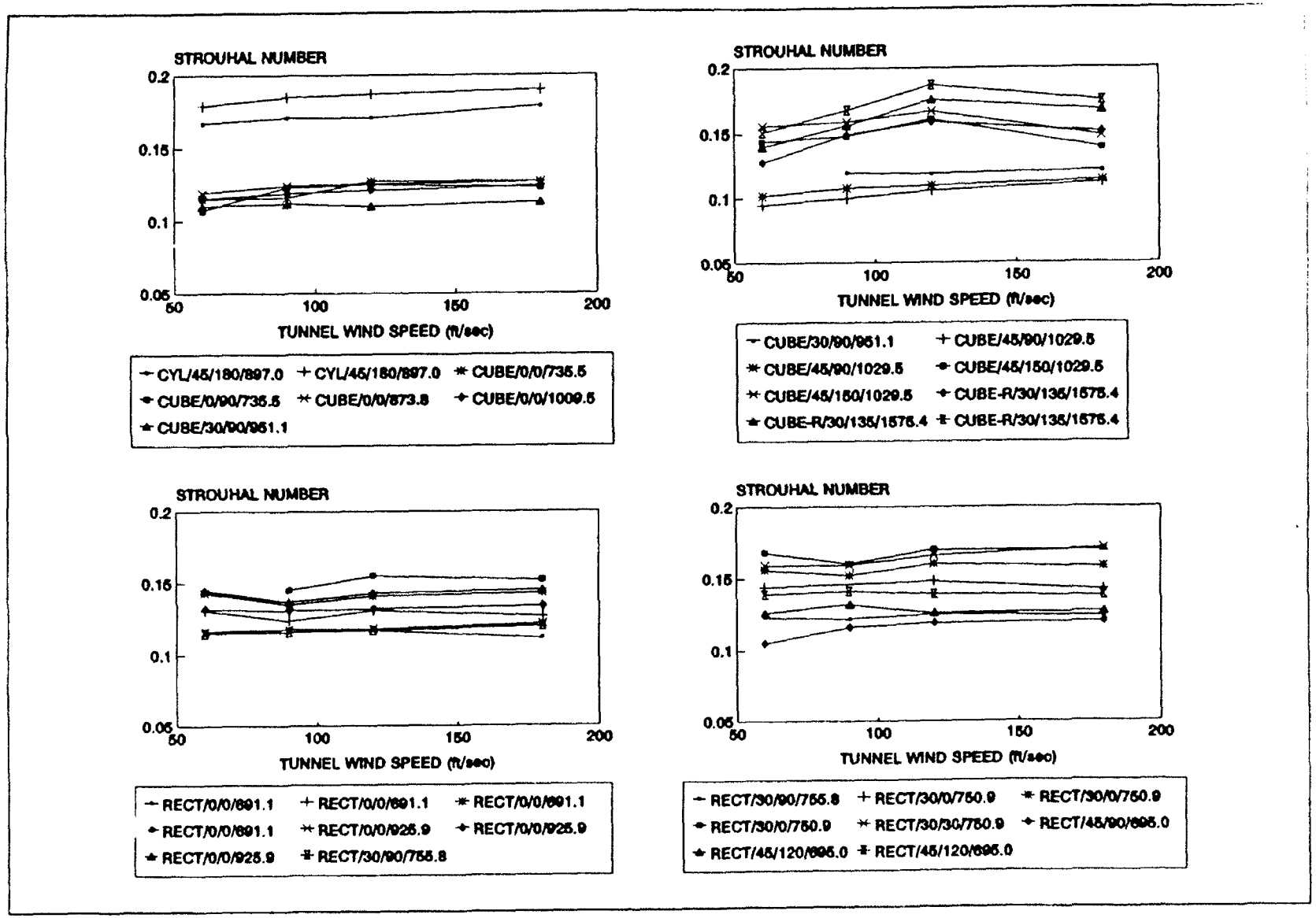

Figure 25. Strouhal data summary. Legends refer to test object shape/declination/azimuth/weight.

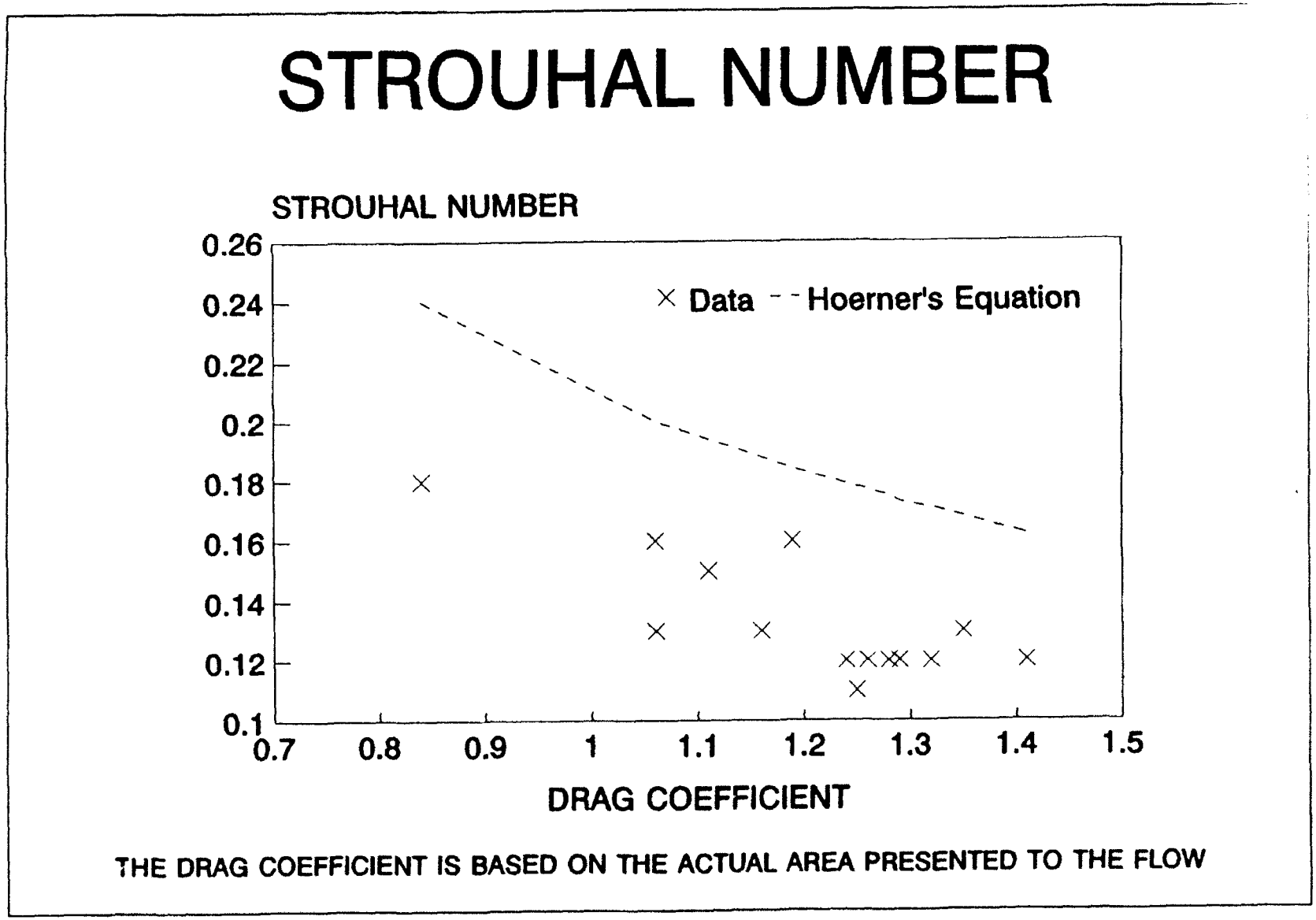

Figure 26. Strouhal data and drag coefficient summary.

Table 3. Strouhal number and drag coefficient specifics.

SHAPE	DECLINATION (degrees)	AZIMUTH (degrees)	WEIGHT (grams)	DRAG COEFF	STROUHAL
CYLINDER	45	180	897.0	0.84	0.18
RECT	45	120	695.0	1.06	0.13
R'ND CUBE	30	135	1575.4	1.06	0.16
CUBE	45	150	1029.5	1.11	0.15
RECT	0	0	925.9	1.16	0.13
RECT	30	0	750.9	1.19	0.16
RECT	30	30	750.9	1.19	0.16
CUBE	0	90	735.5	1.24	0.12
CUBE	45	90	1029.5	1.25	0.11
CUBE	0	0	735.5	1.26	0.12
CUBE	30	90	951.1	1.28	0.12
CUBE	0	0	873.8	1.29	0.12
RECT	45	90	695.0	1.29	0.12
CUBE	0	0	1009.5	1.32	0.12
RECT	0	0	691.1	1.35	0.13
RECT	30	90	755.8	1.41	0.12

4.4 SHEDDING COEFFICIENTS

As vortices are shed from the test object a circulation is established about the test object as shown in Figure 27. With each vortex shed the direction of the circulation reverses. When the wind is superimposed with the circulation a force is generated just as an aircraft wing generates a lift force. Since the circulation about the test object is constantly changing direction with each vortex shed the direction of the force generated undergoes a reversal.

To determine a force or moment coefficient due to shedding requires that the area under the PSD plot be calculated. As seen in the spectrum plots of Section 4.2, the shedding at any particular wind tunnel velocity usually occurs over a band of frequencies instead of at a single frequency. Thus the bandwidth used to calculate a shedding coefficient will affect the value of the coefficient. A quasi-objective determination of bandwidth was made using the Strouhal number equation as follows. First, for a given tunnel velocity, the upper and lower frequency boundries of the bandwidth were subjectively determined by studying the PSD plot for a given test configuration at a given tunnel wind speed. The upper and lower boundries were then used to calculate an upper and lower Strouhal number. The upper and lower Strouhal numbers were then treated as a constant and used to calculate the upper and lower frequencies of the bandwidths at the other wind speeds. If the resulting calculated bandwidth for a particular wind speed did not appear to fit the shedding spectrum at that speed then the upper and lower frequencies were adjusted to fit and these new frequencies were used to repeat the entire process for the other wind speeds. The process was stopped when the calculated bandwidths satisfactorily covered the shedding frequencies.

Figure 28 is a summary chart for the shedding force coefficient for the very good shedding cases indicated in Table 1. Unlike the coefficients shown in the PSD plots which were normalized by a single area, the coefficients shown in Figure 28 are normalized to the actual area over which the forces act. For the cases where the azimuthal angles were 0 and 180 deg the forces acting on the lateral face were responsible for the shedding coefficients. For the 90-deg case the forces acting on the normal face were responsible for the shedding coefficients. In general for the 0-, 90-, and 180-deg cases the coefficients are in the range 0.10 to 0.15 for the force coefficients and 0.10 to 0.20 for the moment coefficients. For cases at other azimuthal angles the vortex shedding resulted in forces acting on both the normal and lateral faces. In these cases the coefficients were less then when the shedding acted on only one face.

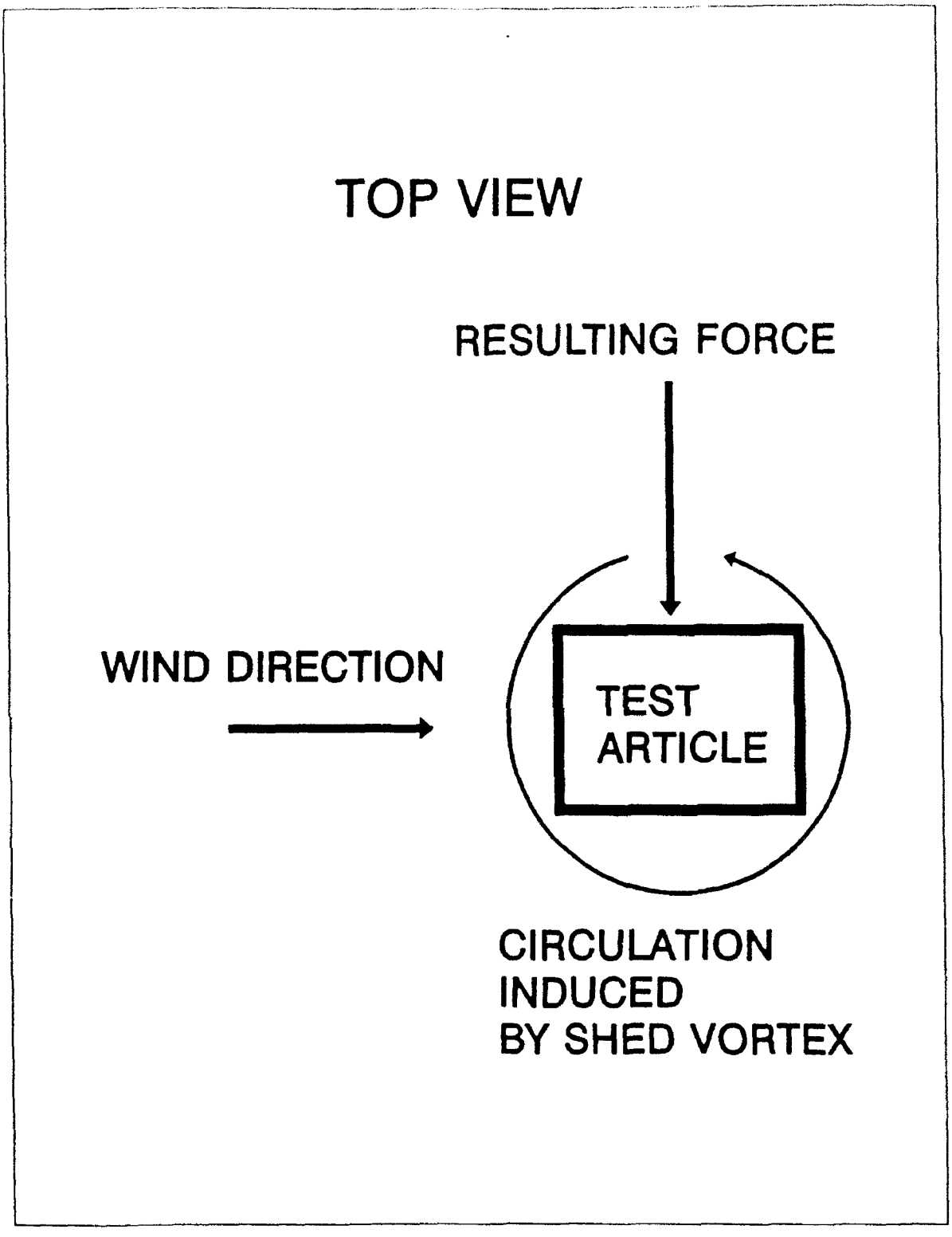

Figure 27. Circulation established around test article by shed vortex causes side forces.

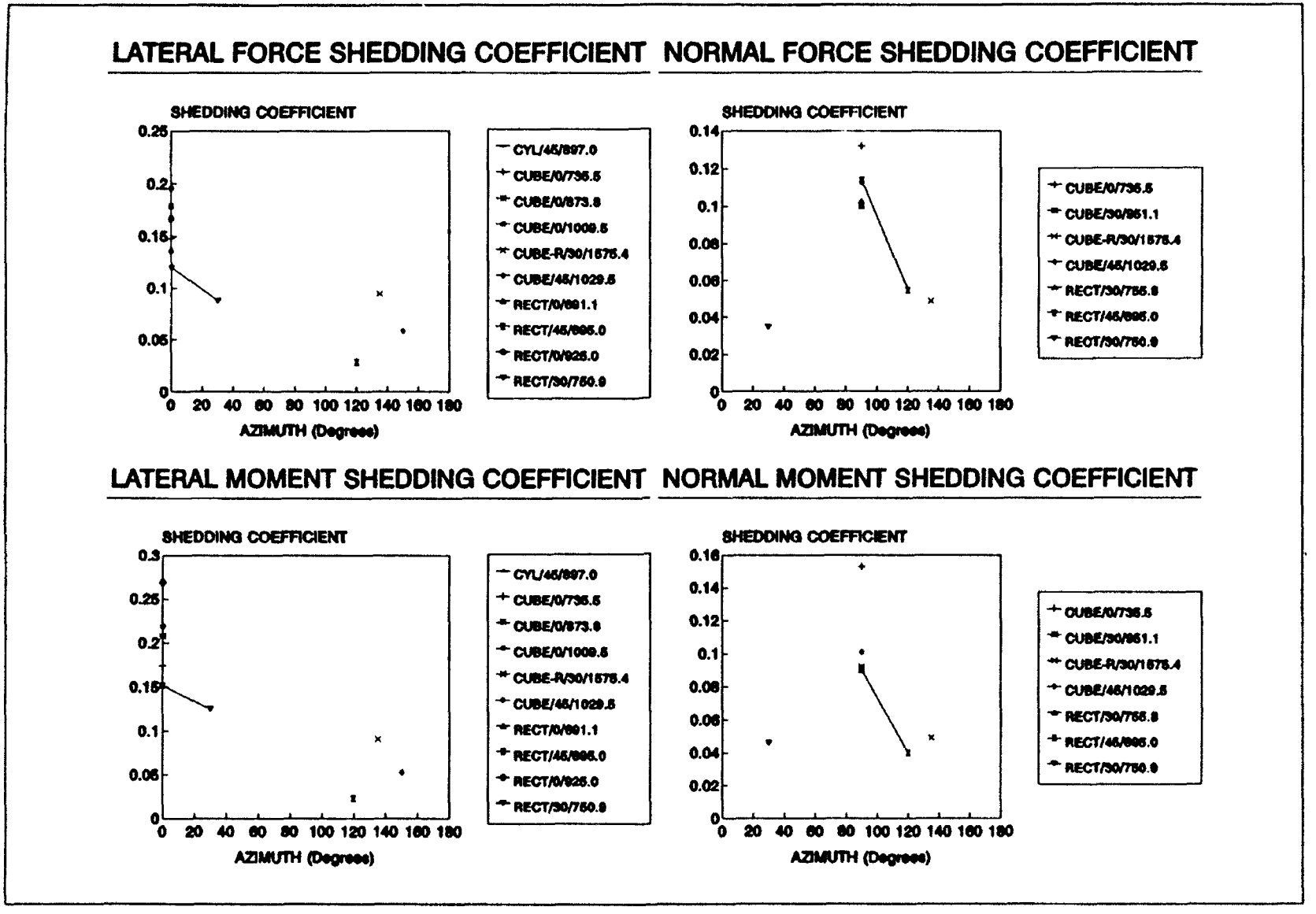

Figure 28. Shedding data summary. Legends refer to test object shape/declination/weight. Data averaged over all wind speeds.

5.0 CONCLUSIONS AND RECOMMENDATIONS

This report examined the results of a wind tunnel experiment designed to simulate the shedding of vortices by a large telescope system. Of the 113 combinations of test shape, declination, and azimuth, only 16 were found to be of a quality suitable for a complete analysis consisting of mean coefficient, spectral analysis, Strouhal number, and shedding coefficient. Sixteen other combinations were found to be likely to yield an incomplete analysis and as a result were analyzed for mean coefficient and PSD but were not analyzed for Strouhal number or shedding coefficient. Another 17 were found to be useful only in a qualitative sense when examined for Strouhal number and shedding coefficient. The remaining 65 combinations were of no use in analyzing shedding.

In general, the quality of the shedding was either poor or nonexistent for cylindrical and near cylindrical (octagon and hexagon) shapes. It would appear that the best shedding occurred for the rectangles and cubes with sharp edges. The two cubes which had rounded edges yielded less distinct shedding frequencies than their counterparts with sharp edges. Finally, the best shedding data tended to occur when the rear surface was perpendicular to the flow. This may have enhanced the flow separation and allowed for a more distinct shed vortex.

The mean force and moment coefficients showed strong dependence on wind angle and little dependency on tunnel wind speed. Characteristically the Reynolds number region between $5x10^5$ and $1x10^6$ displays a transition in which the mean coefficients drop significantly. The lack of such a drop in the data suggests that the experimental conditions did not reach the transition zone.

The Strouhal number analysis showed that the Strouhal number behaved inversely with the drag coefficient. This behavior has been seen by other researchers and these data are quantitatively similar to the values reported elsewhere.

The magnitude of the force and moment coefficients caused by the shedding of vortices is generally 0.1 to 0.2 when the normalizing area is the area over which the forces actually act.

Based on the results of this analysis several recommendations can be made for further analysis and for future data collection and analysis efforts in this area. With respects to further analysis of the data, it is recommended that some more work be done with the transfer function and coherency function analyses to see if such analyses can help separate the signal and noise in the category B, good, data. Regardless of the results of these analyses the category B data should be combed for whatever useful information can be found. For future analysis it is recommended that the normalizing area used to compute coefficients be the actual areas and not a fixed area. The use of a fixed area can distort the data and hide the underlying physical relationships. For future data collection efforts it is recommended that the sample size be at least four times as long.

By enlarging the sample size, the computed transfer functions and coherency functions will be more reliable and may be more likely to separate signal from noise. Finally, future data collection efforts should include near-real time data analysis to help control the quality of the data and point out possible problems while there is an opportunity to correct them.

REFERENCES

1. Jumper, E.J., Mart, P., Lamberson, S., Gates, G., and Bertin, J.J., "Time-Resolved Force and Moment Measurements on a Cubic Body in a Cross Flow: Implications to Wind-Induced Jitter of Telescopes," AIAA-91-0554, American Institute of Aeronautics and Astronautics, Reno, Nevada, 29th Aerospace Sciences Meeting, January 7-10, 1991.

2. Griffin, O.M. and Hall, M.S., "Review - Vortex Shedding Lock-on and Flow Control in Bluff Body Wakes," Transactions of the ASME, Vol. 113, pp. 526-537, December 1991.

3. Roshko, A., "Experiments on the Flow Past a Circular Cylinder at Very High Reynolds Number," Journal of Fluid Mechanics, Vol. 10, pp. 345-356, February 1961.

4. Ayoub, A. and Karamcheti, K., "An Experiment on the Flow Past a Finite Circular Cylinder at High Subcritical and Supercritical Reynolds Numbers," Journal of Fluid Mechanics, Vol. 118, pp. 1-26, May 1982.

5. Gerich, D. and Eckelmann, H., "Influence of End Plates and Free Ends on the Shedding Frequency of Circular Cylinders," Journal of Fluid Mechanics, Vol. 122, pp. 109-121, September 1982.

6. Eisenlohr, H. and Eckelmann, H., "Vortex Splitting and its Consequences in the Vortex Street Wake of Cylinders at Low Reynolds Number," Physical Fluids A, Vol. 1, pp. 189-192, February 1989.

7. Williamson, C.H.K., "Oblique and Parallel Modes of Vortex Shedding in the Wake of a Circular Cylinder at Low Reynolds Numbers," Journal of Fluid Mechanics, Vol. 206, pp. 579-627, September 1989.

8. König, M., Eisenlohr, H., and Eckelmann, H., "The Fine Structure in the Strouhal-Reynolds Number Relationship of the Laminar Wake of a Circular Cylinder," Physical Fluids A, Vol. 2, pp. 1607-1614, September 1990.

9. Stäger, R. and Eckelmann, H., "The Effect of Endplates on the Shedding Frequency of Circular Cylinders in the Irregular Range," Physical Fluids A, Vol. 3, pp. 2116-2121, September 1991.